Downlink Resource Optimization in Multi-STAR-RIS-Assisted MIMO Networks

Qijie Liu, Jian Zhao, *Senior Member, IEEE*, Furao Shen, *Member, IEEE*, Jingon Joung, *Senior Member, IEEE*, and Sumei Sun, *Fellow, IEEE*

***Abstract*— Simultaneously transmitting and reflecting reconfigurable intelligent surfaces (STAR-RISs) enables full-space manipulation of signal propagation. In this work, we consider a multi-STAR-RIS-assisted multiple-input multiple-output (MIMO) system for multi-users and investigate the impact of different STAR-RIS schemes on the system performance. We jointly optimize the beamforming matrix of the base station and the transmitting and reflecting coefficient (TRC) matrix of each STAR-RIS to maximize the sum rate of users. We propose a block coordinate descent (BCD) algorithm to optimize the beamforming matrix and the TRC matrices. We reformulate the optimization problem and optimize the beamforming matrix using the Lagrange duality method to reduce the computational complexity and then employ the constrained concave-convex procedure to tackle the optimization problem for the TRC matrices. When the energy splitting (ES) scheme is applied, our proposed method achieves a remarkable improvement of up to 17.97% in the user sum rate compared to the mode switching and the equal ES schemes in the multi-STAR-RIS-assisted system. Furthermore, when compared with systems assisted by multiple conventional RISs, our system can achieve a substantial gain of 38.99%. The improvement is even more pronounced compared to systems with a single STAR-RIS or a single conventional RIS.**

***Index Terms*— Resource allocation, simultaneous transmitting and reflecting, reconfigurable intelligent surfaces, multiple-input multiple-output (MIMO), sum rate maximization.**

I. Introduction

With the gradual maturity of the fifth-generation (5G) wireless communication technology, more and more research is turning to the upcoming beyond 5G (B5G) and sixth-generation (6G) wireless network communications in order to meet the higher requirements in terms of spectrum efficiency and energy efficiency, microsecond-level latency, and full-dimensional network coverage [1], [2]. These challenging technology requirements necessitate the development of new communication modes [3]. For example, metasurface is considered as a promising enabling technology for B5G and 6G wireless communications. Reconfigurable intelligent surface (RIS), which is a type of metasurface, has gained significant attention from both academia and industry in recent years. RIS is a two-dimensional artificial surface that consists of a large number of low-cost passive element devices. Each element can independently adjust the phase shift of the incident signals, enabling collaborative signal reflection and three-dimensional passive beamforming. The vision of the RIS technology is to create a smart radio environment (SRE) [4], [5], [6], where the wireless propagation conditions can be controlled by physical-layer signaling.

RIS has the potential to revolutionize communication technologies by offering cost-effective and energy-efficient solutions for improving wireless communications; however, conventional RIS functionality is limited to scenarios where both the transmitter and receiver are located on the same side of the RIS. To tackle this issue, simultaneously transmitting and reflecting RIS (STAR-RIS), also known as intelligent omni-surface (IOS), has been proposed [7], [8]. This novel concept overcomes the single-side operation limit of the conventional RIS and attains full spatial coverage. The incident signals of a STAR-RIS element are divided into two parts [9]: reflected signals and transmitted signals. The reflected signals bounce back into the same space as the incident signals. In contrast, the transmitted signals penetrate through the surface and are transmitted to the opposite side of the incident signal space. By adjusting the transmitting and reflecting coefficients (TRCs), STAR-RIS offers additional flexibility for wireless communication system design, potentially enhancing the overall system performance. Considering that each element of a STAR-RIS can dynamically adjust its TRC,the STAR-RIS operation can be categorized into three schemes [10]: i) the energy splitting (ES) scheme, ii) the mode switch (MS) scheme, and iii) the time switch (TS) scheme, as depicted in Fig. 1. In the ES scheme, each element can *simultaneously* transmit and reflect signals, allowing dynamic adjustment of the TRCs. Therefore, greater flexibility in wireless communication can be achieved. In the MS scheme, each element can only operate in a single state, either reflective or transmissive, which is easier to implement but cannot achieve the full-space

Manuscript received 7 January 2024; revised 6 May 2024; accepted 11 June 2024. Date of publication 24 June 2024; date of current version 19 December 2024. This work was supported in part by the Jiangsu Provincial Key R&D Program under Grant BE2023031, and in part by the National Natural Science Foundation of China under Grant 62276127. The work of Jingon Joung was supported in part by the National Research Foundation of Korea (NRF) grant funded by the MSIT under Grant 2022R1A2C1003750. The associate editor coordinating the review of this article and approving it for publication was A. García Armada. *(Corresponding authors: Jian Zhao; Furao Shen.)*

Qijie Liu and Jian Zhao are with the School of Electronic Science and Engineering, Nanjing University, Nanjing 210023, China (e-mail: qijie_liu@smail.nju.edu.cn; jianzhao@nju.edu.cn).

Furao Shen is with the State Key Laboratory for Novel Software Technology and the School of Artificial Intelligence, Nanjing University, Nanjing 210023, China (e-mail: frshen@nju.edu.cn).

Jingon Joung is with the School of Electrical and Electronics Engineering, Chung-Ang University, Seoul 06974, South Korea (e-mail: jgjoung@cau.ac.kr).

Sumei Sun is with the Institute for Infocomm Research, A*STAR, Singapore 138632 (e-mail: sunsm@i2r.a-star.edu.sg).

Color versions of one or more figures in this article are available at https://doi.org/10.1109/TCOMM.2024.3418910.

Digital Object Identifier 10.1109/TCOMM.2024.3418910

0090-6778 © 2024 IEEE. Personal use is permitted, but republication/redistribution requires IEEE permission.
See https://www.ieee.org/publications/rights/index.html for more information.

Authorized licensed use limited to: Nanjing University. Downloaded on March 10,2026 at 07:06:34 UTC from IEEE Xplore. Restrictions apply.

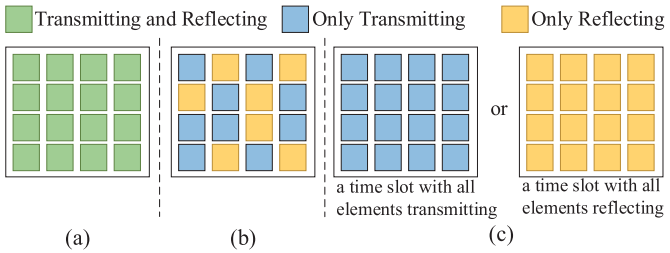

Fig. 1. Three operating schemes of STAR-RIS. (a) Energy splitting (ES) scheme, (b) Mode switch (MS) scheme. (c) Time switch (TS) scheme.

gain as the ES scheme. In the TS scheme, the STAR-RIS operates in either full reflection or full transmission states in a certain time slot. The TS scheme achieves decoupling of the TRCs in the time domain, but it cannot achieve the full-space gain either and has higher requirements for synchronization. One of the three operating schemes can be selected according to the required service in wireless networks. Despite offering increased flexibility and controllability compared to conventional RISs, the study of STAR-RISs is still relatively limited to date. Therefore, this work aims to investigate the applications of STAR-RISs in multiple-input multiple-output (MIMO) wireless networks while considering different operating schemes.

A. Prior Studies

1) Conventional RIS-Assisted Networks: Passive reflective surfaces have found extensive applications in radar, remote sensing, and satellite systems, with emerging utilization in mobile communication systems recently [11], [12]. Research on RIS in wireless communications has focused on active and passive beamforming design, channel estimation, and reliability analysis. The authors of [13] optimized the active beamforming of a base station (BS) and the passive beamforming of the RIS to maximize the weighted sum rate of the downlink. In [14], a two-stage algorithm was proposed to estimate the cascaded channels between the transmitter, the RIS, and the receiver. A modified block coordinate descent algorithm (BCD) was proposed to design near-optimal phase shift values for the RIS in [15]. In [16], the BS intentionally transmitted artificial noise through the RIS to interfere with the eavesdropper, thereby enhancing physical layer security. The uplink weighted sum-rate maximization problem involving both the primary and IoT transmissions for a symbiotic radio system was investigated in [17]. The authors of [18] proposed an convex approximation method to jointly design the active and passive beamforming in an RIS-empowered non-orthogonal multiple access (NOMA) network. The research of optimal RIS placement and orientation in wireless networks is also an important topic. In [19], the authors addressed an RIS placement optimization problem aimed at maximizing the cell coverage by optimizing the RIS orientation and horizontal distance. They derived a closed-form optimal RIS orientation expression. Meanwhile, the authors of [20] considered minimum spacing constraints in a multiple RIS scenario. The utilized genetic algorithms to optimize the deployment positions of multiple RISs.

2) STAR-RIS-Assisted Networks: STAR-RIS is proposed to address the limitations of conventional RIS. Thanks to the breakthroughs in metasurface material technology, STAR-RIS can be implemented using various metasurface-based designs [21], [22]. In [9], a general hardware model, as well as the near- and far-field channel models, were presented for STAR-RIS. The sum rate maximization problem of a full-duplex communication system assisted by a STAR-RIS was investigated in [23]. By optimizing the TRC matrices of the STAR-RIS and selecting the operating schemes, the STAR-RIS-based full-duplex system outperformed the conventional RIS system. In [24], a BCD algorithm was proposed to maximize the sum rate in a STAR-RIS-assisted MIMO communication system, and various operating schemes were compared. The authors of [24] considered the joint optimization of STAR-RIS positions and beamforming in a wireless network to maximize the user rates, where they proposed an alternating optimization algorithm to solve this problem.

The authors of [25] compared the orthogonal multiple access (OMA) and NOMA schemes in a STAR-RIS-assisted wireless communication network, and they showed that the NOMA scheme was superior to the OMA scheme in such a system. The authors of [26] investigated a STAR-RIS-assisted multi-user downlink MISO communication system, where they proposed a hybrid reinforcement learning (RL) algorithm to jointly optimize the active and passive beamforming to solve the high-dimensional mixed continuous and discrete problems caused by the coupled phase shifts. In [27], the trajectory and the active beamforming of an unmanned aerial vehicle (UAV) were jointly optimized with the TRC matrices of the STAR-RIS to maximize the sum rate of users, where an RL-based algorithm was employed to circumvent the high computational complexity in the STAR-RIS coefficient optimization.

B. Motivation and Contribution

Current research on STAR-RIS primarily focuses on wireless systems assisted by a single STAR-RIS [23], [28]. Although STAR-RIS can provide wireless communication services with an entire 360° coverage, the effective service range of a single STAR-RIS is still limited. Given the vast potentials of the RIS and STAR-RIS in the next-generation communication systems, we consider a more realistic scenario with *multiple* STAR-RIS collaborations and we summarize the main contributions of this paper as follows:

- This study first proposes a multi-STAR-RIS-assisted MIMO communication system model. With the novel model, a sum rate maximization problem is formulated and solved by jointly optimizing the coupled beamforming matrix of the BS and the TRC matrices of all STAR-RISs under non-convex constraints. Optimizing the coupled matrices is nontrivial and the optimization problem is challenging.
- To address these challenges, the beamforming matrix and the TRC matrices are alternately optimized by decoupling the beamforming and TRC matrices through a BCD algorithm. Firstly, we reformulate the non-convex

Authorized licensed use limited to: Nanjing University. Downloaded on March 10,2026 at 07:06:34 UTC from IEEE Xplore. Restrictions apply.

objective function through a weighted minimum mean square error (WMMSE) algorithm. Then, we use the Lagrange duality method to find the optimal beamforming matrix through a bisection method to reduce the computational complexity. Finally, to tackle the mutually coupled TRC matrices of multiple STAR-RISs, we decouple the variables and introduce auxiliary variables in the problem to enable the constrained concave-convex procedure (CCCP) for optimization.

- The numerical results verify the efficacy of the proposed algorithm. The performance of various operating schemes of STAR-RISs is evaluated. Further numerical comparisons show that the proposed method significantly enhances the communication performance of systems with multiple STAR-RISs.
- We provide detailed analysis for: i) the convergence of the proposed scheme, ii) the empirical cumulative distribution function (CDF) of the sum rate under different schemes, and iii) the impact of the transmit power and the number of STAR-RIS elements on system performance. In addition, we show that a multi-STAR-RIS-assisted communication system can be effectively optimized under various operating schemes.

C. Organization and Notation

The rest of this paper is organized as follows. Section II presents the system model considered in this study. In Section III, the optimization problem is presented based on the system model and reformulated by utilizing the WMMSE method. Section IV proposes an algorithm for solving the reformulated problem, including optimizing the beamforming matrix and the TRC matrices. Section V provides numerical results that compare systems using different STAR-RIS and conventional RIS schemes to verify the performance of the proposed methods. Section VI draws the conclusion of this study.

Notations: In this paper, lower- and upper-case boldface letters denote vectors and matrix, respectively. $\mathbb{C}^{M\times 1}$ denotes an M-dimensional complex vector and $\mathbb{C}^{M\times N}$ represent an $M\times N$ dimensional complex matrix. For two matrix $\mathbf{A}$ and $\mathbf{B}$, $\mathbf{A}\odot\mathbf{B}$ denotes the Hadamard product of them. $|\mathbf{A}|$ and $\mathrm{Tr}\,(.)$ represent the determinant and trace operation of $\mathbf{A}$. $(.)^{\mathsf{T}}$ and $(.)^{H}$ denote the transpose and conjugate transpose operations, respectively. $\mathrm{diag}\,(\mathbf{a})$ returns a diagonal square matrix with the elements of vector $\mathbf{a}$ on its main diagonal, while $\mathrm{diag}\,(\mathbf{A})$ returns a column vector composed of the main diagonal elements of $\mathbf{A}$. $\mathbf{I}_N$ denotes an identity matrix of size $N\times N$, and $\mathbf{1}_N$ is a length-N vector with all one elements. $\mathcal{CN}\left(\mathbf{0},\sigma^2\mathbf{I}\right)$ denotes a circularly symmetric complex normal zero-mean random vector, whose covariance matrix is $\sigma^2\mathbf{I}$. $\Re\{.\}$ returns the real component of a complex argument.

II. System Model

This section describes a multi-STAR-RIS-assisted MIMO communication system in which the BS and multiple STAR-RISs work together to serve multiple users with multiple antennas. The following subsections introduce the basic STAR-RIS operation, the channel, and the signal models.

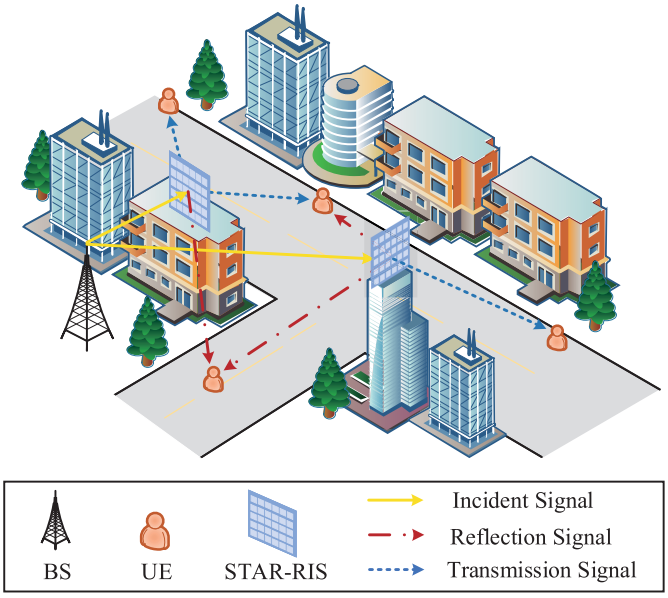

Fig. 2. System model of multi-STAR-RIS-assisted MIMO wireless network.

A. System Description

As shown in Fig. 2, we consider a multi-STAR-RIS-assisted MIMO communication scenario with one BS, K users, and L STAR-RISs. The BS is equipped with N_{B} antennas, each user has N_{U} receive antennas, and each STAR-RIS consists of M passive elements that reflect or transmit the signals coming from the BS towards the users. To consider a practical communication scenario of STAR-RISs, we assume that the direct link from the BS to all users has been blocked by obstacles and focus on enhancing user services facilitated by all STAR-RISs.

B. Basic STAR-RIS Operation Model

In this paper, we assume the operating scheme of each STAR-RIS is configured as the ES mode. According to the introduction in Section I, the ES scheme has higher flexibility in adjusting the communication environment and improving communication system quality compared to other operating schemes. Let $\mathcal{L}=\{1,2,\cdots,L\}$ and $\mathcal{M}=\{1,2,\cdots,M\}$ represent the set of STAR-RISs and the set of elements for each STAR-RIS, respectively.

The TRCs of the mth element of the lth STAR-RIS are denoted as $\sqrt{\beta^{\mathrm{t}}_{m,l}}e^{j\phi^{\mathrm{t}}_{m,l}}$ and $\sqrt{\beta^{\mathrm{r}}_{m,l}}e^{j\phi^{\mathrm{r}}_{m,l}}$ respectively, where $m\in\mathcal{M}$ and $l\in\mathcal{L}$. Here, $\beta^{\mathrm{t}}_{m,l}\in[0,1]$, $\phi^{\mathrm{t}}_{m,l}\in[0,2\pi)$, $\beta^{\mathrm{r}}_{m,l}\in[0,1]$, and $\phi^{\mathrm{r}}_{m,l}\in[0,2\pi)$ represent the transmitting and reflecting squared amplitudes and phase shift responses of the mth element of the lth STAR-RIS, respectively. It is assumed that the surface electric and magnetic impedance of the STAR-RIS can be adjusted, allowing for independent selection of $\phi^{\mathrm{t}}_{m,l}$ and $\phi^{\mathrm{r}}_{m,l}$. However, the TRCs must satisfy the energy conservation constraint $\beta^{\mathrm{t}}_{m,l}+\beta^{\mathrm{r}}_{m,l}=1,\forall m\in\mathcal{M}$, $l\in\mathcal{L}$.

Thus, the diagonal TRC matrix of the lth STAR-RIS can be denoted by $\mathbf{\Phi}^{l}_{\xi}=\mathrm{diag}\left(\sqrt{\beta^{\xi}_{1,l}}e^{j\phi^{\xi}_{1,l}},\cdots,\sqrt{\beta^{\xi}_{M,l}}e^{j\phi^{\xi}_{M,l}}\right)\in\mathbb{C}^{M\times M}$, where $\xi\in\{\mathrm{t},\mathrm{r}\}$ indicate whether the user is

Authorized licensed use limited to: Nanjing University. Downloaded on March 10,2026 at 07:06:34 UTC from IEEE Xplore. Restrictions apply.

in the transmission or the reflection side with respect to the lth STAR-RIS.

For a given user k, it may be on the transmission side of some STAR-RISs, while on the reflection side of other STAR-RISs. However, once the position of the kth user is fixed, whether it is on the transmission or reflection side of the lth STAR-RIS is also determined. Therefore, we can construct an equivalent TRC matrix $\mathbf{Q}_k \in \mathbb{C}^{LM\times LM}$ for the kth user considering its relative position with respective to all the STAR-RISs, i.e.,

$$\mathbf{Q}_k = \mathrm{Diag}\left(\mathbf{\Phi}_\xi^1, \cdots, \mathbf{\Phi}_\xi^L\right), \tag{1}$$

where $\mathrm{Diag}(\cdot)$ returns a block diagonal matrix made by aligning the input matrices along its diagonal.

C. Signal Model

The channel from the BS to the lth STAR-RIS and the channel from the lth STAR-RIS to the kth user are denoted by $\mathbf{F}_l \in \mathbb{C}^{M\times N_\mathrm{B}}$ and $\mathbf{H}_k^l \in \mathbb{C}^{N_\mathrm{U}\times M}$, respectively. Since the locations of the BS and the STAR-RIS are fixed, we use $\mathbf{F} = [\mathbf{F}_1, \mathbf{F}_2, \cdots, \mathbf{F}_L]^H \in \mathbb{C}^{LM\times N_\mathrm{B}}$ to represent the channel from the BS to all STAR-RISs. Similarly, the channel from all STAR-RISs to the kth user is denoted as $\mathbf{H}_k = \left[\mathbf{H}_k^1, \mathbf{H}_k^2, \cdots, \mathbf{H}_k^L\right] \in \mathbb{C}^{N_\mathrm{U}\times LM}$ once we know the position of the kth user.

We denote the symbol vector and the active beamforming matrix for the kth user at the BS by $\mathbf{s}_k \in \mathbb{C}^{N_\mathrm{U}\times 1}$ and $\mathbf{V}_k \in \mathbb{C}^{N_\mathrm{B}\times N_\mathrm{U}}$, respectively. The signal transmitted from the BS can be expressed as

$$\mathbf{x} = \sum_{k=1}^{K} \mathbf{V}_k \mathbf{s}_k. \tag{2}$$

Thus, the signal received by the kth user is given as

$$\begin{aligned}\mathbf{y}_k &= \mathbf{H}_k\mathbf{Q}_k\mathbf{F}\mathbf{x} + \mathbf{n}_k \\ &= \underbrace{\mathbf{H}_k\mathbf{Q}_k\mathbf{F}\mathbf{V}_k\mathbf{s}_k}_{\text{Desired signal}} + \underbrace{\sum_{k'\neq k}^{K} \mathbf{H}_k\mathbf{Q}_k\mathbf{F}\mathbf{V}_{k'}\mathbf{s}_{k'}}_{\text{Inter-user interference}} + \mathbf{n}_k,\end{aligned} \tag{3}$$

where $\mathbf{n}_k \in \mathbb{C}^{N_\mathrm{U}\times 1}$ is the noise vector at the kth user with $\mathbf{n}_k \sim \mathcal{CN}\left(\mathbf{0}, \sigma_k^2\mathbf{I}\right)$, and σ_k^2 is the noise power of the kth user.

Here, we denote $\overline{\mathbf{H}}_k = \mathbf{H}_k\mathbf{Q}_k\mathbf{F}_k/\sigma_k \in \mathbb{C}^{N_\mathrm{U}\times N_\mathrm{U}}$ for simplicity. The achievable rate for the kth user can be written as

$$R_k = \log\left|\mathbf{I}_{N_\mathrm{U}} + \overline{\mathbf{H}}_k\mathbf{V}_k\mathbf{V}_k^H\overline{\mathbf{H}}_k^H\mathbf{C}_k^{-1}\right|, \tag{4}$$

where $\mathbf{C}_k \in \mathbb{C}^{N_\mathrm{U}\times N_\mathrm{U}}$ is the interference plus noise covariance matrix of the kth user and can be written as

$$\mathbf{C}_k = \sum_{k'\neq k}^{K} \overline{\mathbf{H}}_k\mathbf{V}_{k'}\mathbf{V}_{k'}^H\overline{\mathbf{H}}_k^H + \mathbf{I}_{N_\mathrm{U}}. \tag{5}$$

III. Problem Formulation

In this section, we formulate the optimization problem based on the system model given in Section II and analyze the objective function and the constraints of the optimization problem. Then, we transform the objective function of the originally non-convex problem using the WMMSE method, facilitating its subsequent solution through the BCD algorithm.

A. Problem Formulation

We aim to maximize the sum rate of all users by jointly optimizing the beamforming matrix $\mathbf{V}_k$ for the BS and the TRC matrix $\mathbf{Q}_k$. The sum rate of all users is $R = \sum_{k=1}^{K} R_k$ where R_k is given in (4). Therefore, the optimization problem can be formulated as

$$\underset{\mathbf{V}_k,\mathbf{Q}_k}{\text{maximize}} \sum_{k=1}^{K} R_k \tag{6a}$$

$$\text{s.t.} \sum_{k=1}^{K} \mathrm{Tr}\left(\mathbf{V}_k\mathbf{V}_k^H\right) \le P_{\max}, \tag{6b}$$

$$\mathbf{Q}_k = \mathrm{Diag}\left(\mathbf{\Phi}_\xi^1, \cdots, \mathbf{\Phi}_\xi^L\right), \ \forall k \in \mathcal{K}, \tag{6c}$$

$$[\mathbf{\Phi}_\xi^l]_m = \sqrt{\beta_{m,l}^\xi}e^{j\phi_{m,l}^\xi}, \ \xi = \{\mathrm{t}, \mathrm{r}\}, \tag{6d}$$

$$\beta_{m,l}^\xi \in [0,1], \ \phi_{m,l}^\xi \in [0, 2\pi), \tag{6e}$$

$$\beta_{m,l}^\mathrm{t} + \beta_{m,l}^\mathrm{r} = 1, \ \forall m \in \mathcal{M}, \ l \in \mathcal{L}. \tag{6f}$$

Here, the constraint (6b) is the maximum power constraint for the BS; (6c) to (6f) are the constraints for optimizing the TRCs; (6c) is the equivalent TRC matrix, which takes into account the relative position between the kth user and all the STAR-RISs; (6d) to (6f) are constraints for the ES scheme of STAR-RISs.

B. Reformulation of the Proposed Problem

Problem (6) is apparently a non-convex problem because of the non-convex objective function and the non-convex constraints. To tackle this problem, we utilize the WMMSE algorithm [29] to reformulate it. We consider a linear decoding matrix so that the estimated signal vector of each user is given by

$$\hat{\mathbf{s}}_k = \mathbf{U}_k^H\mathbf{y}_k, \quad \forall k \in \mathcal{K}, \tag{7}$$

where $\mathbf{U}_k \in \mathbb{C}^{N_\mathrm{U}\times N_\mathrm{U}}$ is the decoding matrix for the kth user. Since the signal vectors $\mathbf{s}_k$ and the noise $\mathbf{n}_k$ are mutually independent, we can derive the mean square error (MSE) matrix of user k as

$$\mathbf{E}_k = \mathbb{E}_{\mathbf{s},\mathbf{n}}\left[\left(\hat{\mathbf{s}}_k - \mathbf{s}_k\right)\left(\hat{\mathbf{s}}_k - \mathbf{s}_k\right)^H\right] \tag{8a}$$

$$\begin{aligned}&= \mathbf{U}_k^H\left(\mathbf{I}_{N_\mathrm{U}} + \sum_{k'\neq k}^{K} \overline{\mathbf{H}}_k\mathbf{V}_{k'}\mathbf{V}_{k'}^H\overline{\mathbf{H}}_k^H\right)\mathbf{U}_k \\ &\quad + \left(\mathbf{I}_{N_\mathrm{U}} - \mathbf{U}_k^H\overline{\mathbf{H}}_k\mathbf{V}_k\right)\left(\mathbf{I}_{N_\mathrm{U}} - \mathbf{U}_k^H\overline{\mathbf{H}}_k\mathbf{V}_k\right)^H.\end{aligned} \tag{8b}$$

By introducing auxiliary semidefinite matrices $\mathbf{Z}_k \succeq \mathbf{0}$, we can reformulate Problem (6) as follows:

$$\underset{\mathbf{V}_k,\mathbf{Q}_k,\mathbf{U}_k,\mathbf{Z}_k}{\text{maximize}} \sum_{k=1}^{K} f_k\left(\mathbf{V}_k, \mathbf{Q}_k, \mathbf{U}_k, \mathbf{Z}_k\right) \tag{9a}$$

Authorized licensed use limited to: Nanjing University. Downloaded on March 10,2026 at 07:06:34 UTC from IEEE Xplore. Restrictions apply.

$$\text{s.t. } \mathbf{Z}_k \succeq \mathbf{0}, \tag{9b}$$

$$(6b) - (6f), \tag{9c}$$

where $f_k\left(\mathbf{V}_k, \mathbf{Q}_k, \mathbf{U}_k, \mathbf{Z}_k\right)$ is given by

$$f_k\left(\mathbf{V}_k, \mathbf{Q}_k, \mathbf{U}_k, \mathbf{Z}_k\right) = \log\left|\mathbf{Z}_k\right| - \mathrm{Tr}\left(\mathbf{Z}_k \mathbf{E}_k\right) + d_k, \tag{10}$$

and d_k is a constant term. The proof of equivalence between Problem (6) and (9) can be found in [29, Appendix A].

Different from the original objective function of Problem (6), we make it more tractable in Problem (9) by introducing additional optimization variables. Notice that for a given TRC matrix $\mathbf{Q}_k$, $f_k\left(\mathbf{V}_k, \mathbf{Q}_k, \mathbf{U}_k, \mathbf{Z}_k\right)$ is a concave function for each set of optimization variables when any two of the variables $\{\mathbf{V}_k, \mathbf{U}_k, \mathbf{Z}_k\}$ are fixed. Therefore, we utilize the BCD algorithm to solve Problem (9).

We first solve Problem (9) while fixing $\{\mathbf{V}_k, \mathbf{Q}_k, \mathbf{Z}_k\}$. In this case, $f_k\left(\mathbf{V}_k, \mathbf{Q}_k, \mathbf{U}_k, \mathbf{Z}_k\right)$ can be regarded as a function which is only related to $\mathbf{U}_k$. Hence, we can set the first-order derivative of $f_k\left(\mathbf{V}_k, \mathbf{Q}_k, \mathbf{U}_k, \mathbf{Z}_k\right)$ with respect to $\mathbf{U}_k$ to zero, which gives the optimal $\mathbf{U}_k$ as

$$\mathbf{U}_k^{\star} = \left(\overline{\mathbf{H}}_k \mathbf{V}_k \mathbf{V}_k^H \overline{\mathbf{H}}_k^H + \mathbf{C}_k\right)^{-1} \overline{\mathbf{H}}_k \mathbf{V}_k. \tag{11}$$

Then we solve Problem (9) for $\mathbf{Z}_k$ while fixing $\{\mathbf{V}_k, \mathbf{Q}_k, \mathbf{U}_k\}$. Similar to $\mathbf{U}_k$, the optimal $\mathbf{Z}_k$ is given by

$$\mathbf{Z}_k^{\star} = \mathbf{E}_k^{-1}, \tag{12}$$

where $\mathbf{E}_k$ is given in (8),

Different from $\mathbf{U}_k$ and $\mathbf{Z}_k$, there is no closed form solution for $\mathbf{V}_k$ and $\mathbf{Q}_k$. Hence, in the following sections, we focus on optimizing the beamforming matrices $\mathbf{V}_k$ and the TRC matrices $\mathbf{Q}_k$.

IV. Joint Beamforming and TRC Optimization

Based on the reformulation given in Section III, we propose an iterative algorithm to jointly optimize the beamforming matrix and TRC matrices in this section.

A. Optimization of Beamforming Matrix $\mathbf{V}_k$

In this subsection, we mainly focus our attention on optimizing the beamforming matrix $\mathbf{V}_k$ while fixing $\{\mathbf{Q}_k, \mathbf{U}_k, \mathbf{Z}_k\}$. By substituting $\mathbf{E}_k$ into (9a) and removing the constant terms, the objective function (13), as shown at the bottom of the next page.

For simplicity, we introduce auxiliary matrix $\mathbf{A} = \sum_{k'=1}^{K} \overline{\mathbf{H}}_{k'}^H \mathbf{U}_{k'} \mathbf{Z}_{k'} \mathbf{U}_{k'}^H \overline{\mathbf{H}}_{k'}$ and $\mathbf{B}_k = \mathbf{Z}_k \mathbf{U}_k^H \overline{\mathbf{H}}_k$. Hence, the beamforming optimization problem can be rewritten as

$$\underset{\mathbf{V}_k}{\text{minimize}} \sum_{k=1}^{K} \left(\mathrm{Tr}\left(\mathbf{V}_k^H \mathbf{A} \mathbf{V}_k\right) - 2\Re\left\{\mathrm{Tr}\left(\mathbf{B}_k \mathbf{V}_k\right)\right\}\right) \tag{14a}$$

$$\text{s.t. } (6b). \tag{14b}$$

Problem (14) can be reformulated as a second-order cone programming (SOCP) problem, which can be solved using standard convex optimization packages such as CVX [30]. However, solving SOCP problems using those standard optimization packages has low efficiency. Therefore, we propose a closed-form solution for the beamforming optimization problem using the Lagrange duality method, which is much more efficient. Because Problem (14) is a convex problem and satisfies the Slater's condition,[1] it follows that strong duality can be established between Problem (14) and its Lagrangian dual problem. That is, the optimum solution of the dual problem is also the optimum solution of the original problem (14).

Specifically, the Lagrangian of (14) is

$$L\left(\mathbf{V}_k, \lambda\right) = \sum_{k}^{K} \left(\mathrm{Tr}\left(\mathbf{V}_k^H \mathbf{A} \mathbf{V}_k\right) - 2\Re\left\{\mathrm{Tr}\left(\mathbf{B}_k \mathbf{V}_k\right)\right\}\right) + \lambda\left(\sum_{k}^{K} \mathrm{Tr}\left(\mathbf{V}_k \mathbf{V}_k^H\right) - P_{\max}\right), \tag{15}$$

where $\lambda > 0$ is the dual variable associated with the power constraint of the BS.

By setting the first-order derivative of $L\left(\mathbf{V}_k, \lambda\right)$ with respect to $\mathbf{V}_k$ to zero, we obtain the optimal solution of $\mathbf{V}_k$ as

$$\mathbf{V}_k\left(\lambda\right) = \left(\mathbf{A} + \lambda \mathbf{I}_{N_{\mathrm{U}}}\right)^{\dagger} \mathbf{B}_k^H, \tag{16}$$

where $(.)^{\dagger}$ represents the matrix pseudoinverse. Based on the complementary slackness condition for the power constraint, the value of λ needs to satisfy

$$\lambda\left(\sum_{k=1}^{K} \mathrm{Tr}\left(\mathbf{V}_k\left(\lambda\right) \mathbf{V}_k\left(\lambda\right)^H\right) - P_{\max}\right) = 0. \tag{17}$$

The optimal value of λ can be obtained by the bisection search method [31].

B. Optimization of TRC Matrix $\mathbf{Q}_k$

In this subsection, we fix $\{\mathbf{V}_k, \mathbf{U}_k, \mathbf{Z}_k\}$ and focus our attention on the subproblem with respect to $\mathbf{Q}_k$. The problem formulation can be rewritten as

$$\underset{\mathbf{Q}_k}{\text{minimize}} \sum_{k=1}^{K} \left(\mathrm{Tr}\left(\mathbf{V}_k^H \mathbf{A} \mathbf{V}_k\right) - 2\Re\left\{\mathrm{Tr}\left(\mathbf{B}_k \mathbf{V}_k\right)\right\}\right) \tag{18a}$$

$$\text{s.t. } (6b) - (6f). \tag{18b}$$

Problem (18) is a non-convex optimization problem due to the non-convexity of the objective function (18a) and the constraints. To tackle this non-convex problem, we first substitute $\overline{\mathbf{H}}_k = \mathbf{H}_k \mathbf{Q}_k \mathbf{F}_k / \sigma_k$ into the objective function (18a) and we have (19) and (20), as shown at the bottom of the next page. Then, we use the following Lemma to handle the non-convexity of (19) and (20).

Lemma 1 [32]: For any diagonal matrix $\mathbf{D} = \mathrm{diag}\left(d_1, \cdots, d_m\right) \in \mathbb{C}^{m \times m}$, we have

$$\mathrm{Tr}\left(\mathbf{D}^H \mathbf{C}_1 \mathbf{D} \mathbf{C}_2\right) = \mathbf{d}^H \left(\mathbf{C}_1 \odot \mathbf{C}_2^{\mathsf{T}}\right) \mathbf{d}, \tag{21}$$

$$\mathrm{Tr}\left(\mathbf{D}^H \mathbf{C}_2^H\right) = \mathbf{c}_2^H \mathbf{d}, \tag{22}$$

$$\mathrm{Tr}\left(\mathbf{D} \mathbf{C}_2\right) = \mathbf{1}^{\mathsf{T}} \left(\mathbf{D} \odot \mathbf{C}_2^{\mathsf{T}}\right) \mathbf{1} = \mathbf{d}^{\mathsf{T}} \mathbf{c}_2, \tag{23}$$

where $\mathbf{d} = \mathrm{diag}(\mathbf{D})$ and $\mathbf{c}_2 = \mathrm{diag}(\mathbf{C}_2)$.

[1] According to Step 2 in **Algorithm 1**, we can always find a feasible point $\mathbf{V}_k^{(0)}$ that strictly satisfy constraint (6b) so that the Slater's condition holds.

Authorized licensed use limited to: Nanjing University. Downloaded on March 10,2026 at 07:06:34 UTC from IEEE Xplore. Restrictions apply.

According to *Lemma 1*, we can transform (19) and (20) into

$$\sum_{k=1}^{K} \mathrm{Tr}\left(\mathbf{Q}_k^H \mathbf{H}_k^H \mathbf{U}_k \mathbf{Z}_k \mathbf{U}_k^H \mathbf{H}_k \mathbf{Q}_k \mathbf{F} \sum_{k'=1}^{K} \mathbf{V}_{k'} \mathbf{V}_{k'}^H\right) = \sum_{k=1}^{K} \mathbf{q}_k^H \mathbf{G}_k \mathbf{q}_k, \tag{24}$$

and

$$\sum_{k=1}^{K} 2\Re\left\{\mathrm{Tr}\left(\mathbf{Z}_k \mathbf{U}_k^H \mathbf{H}_k \mathbf{Q}_k \mathbf{F} \mathbf{V}_k\right)\right\} = \sum_{k=1}^{K} 2\Re\left\{\mathbf{q}_k^H \mathbf{p}_k\right\}, \tag{25}$$

where $\mathbf{q}_k = \mathrm{diag}(\mathbf{Q}_k)$, $\mathbf{p}_k = \mathrm{diag}\left(\mathbf{F}\mathbf{V}_k \mathbf{Z}_k \mathbf{U}_k^H \mathbf{H}_k\right)$ and $\mathbf{G}_k = \left(\mathbf{H}_k^H \mathbf{U}_k \mathbf{Z}_k \mathbf{U}_k^H \mathbf{H}_k\right) \odot \left(\mathbf{F} \sum_{k'=1}^{K} \mathbf{V}_{k'} \mathbf{V}_{k'}^H\right)^H$.

Based on the above transformation, we can reformulate Problem (18) as

$$\underset{\mathbf{q}_k}{\text{minimize}} \sum_{k=1}^{K} \left(\mathbf{q}_k^H \mathbf{G}_k \mathbf{q}_k / \sigma_k^2 - 2\Re\left\{\mathbf{q}_k^H \mathbf{p}_k\right\} / \sigma_k\right) \tag{26a}$$

$$\text{s.t. } \mathbf{q}_k = \mathrm{diag}(\mathbf{Q}_k), \tag{26b}$$

$$\mathbf{Q}_k = \mathrm{Diag}\left(\mathbf{\Phi}_\xi^1, \cdots, \mathbf{\Phi}_\xi^L\right), \tag{26c}$$

$$\beta_{m,l}^{\xi}, \in [0,1], \tag{26d}$$

$$\beta_{m,l}^{\mathrm{t}} + \beta_{m,l}^{\mathrm{r}} = 1, \ \forall m \in \mathcal{M}, \ l \in \mathcal{L}. \tag{26e}$$

Constraint (26c) represents the equivalent TRC matrix of the kth user considering all the STAR-RISs. The main difficulty in solving Problem (26) is (26e), which shows the transmitting and reflecting TRCs are coupled. Unlike the single STAR-RIS case, the resource allocation involving multiple STAR-RISs is more challenging. This is because each user may be located on the reflection side of one STAR-RIS but on the transmission side of another. Depending on their location, the TRC matrices $\mathbf{Q}_k$ of different users may also be coupled.

In the case of multi-users, this coupling makes it difficult for us to directly use the algorithm proposed in [28] to solve the optimization problem of TRC. Based on the above analysis, we introduce auxiliary variables ζ to reformulate constraint (26e), where $\zeta \in \{\mathrm{t}, \mathrm{r}\}$ and $\zeta = \bar{\xi}$. That is, $\zeta = \mathrm{t}$, when $\xi = \mathrm{r}$; and $\zeta = \mathrm{r}$, otherwise. We define matrix $\widetilde{\mathbf{\Phi}}_\zeta^l$ to represent the TRC matrix with state ζ. Similar to (1), we define $\widetilde{\mathbf{Q}}_k = \mathrm{Diag}\left(\mathbf{\Phi}_\zeta^1, \cdots, \mathbf{\Phi}_\zeta^L\right)$. Hence, we have $\widetilde{\mathbf{q}}_k = \mathrm{diag}\left(\widetilde{\mathbf{Q}}_k\right)$.

Moreover, we introduce $\mathbf{\Theta}_k = \mathbf{q}_k \mathbf{q}_k^H$, and $\widetilde{\mathbf{\Theta}}_k = \widetilde{\mathbf{q}}_k \widetilde{\mathbf{q}}_k^H$. Thereby we can use $\mathrm{diag}\left(\mathbf{\Theta}_k\right)$ to represent the TRCs for user k, while $\mathrm{diag}\left(\widetilde{\mathbf{\Theta}}_k\right)$ represents the opposite state of $\mathrm{diag}\left(\mathbf{\Theta}_k\right)$. Problem (26) can be transformed to

$$\underset{\mathbf{q}_k, \widetilde{\mathbf{q}}_k}{\text{minimize}} \sum_{k=1}^{K} \left(\mathbf{q}_k^H \mathbf{G}_k \mathbf{q}_k / \sigma_k^2 - 2\Re\left\{\mathbf{q}_k^H \mathbf{p}_k\right\} / \sigma_k\right) \tag{27a}$$

$$\text{s.t. } \mathbf{\Theta}_k = \mathbf{q}_k \mathbf{q}_k^H, \widetilde{\mathbf{\Theta}}_k = \widetilde{\mathbf{q}}_k \widetilde{\mathbf{q}}_k^H, \tag{27b}$$

$$\mathrm{diag}\left(\mathbf{\Theta}_k + \widetilde{\mathbf{\Theta}}_k\right) = \mathbf{1}_{LM}. \tag{27c}$$

To handle the non-convex constraint (27b), we use the following lemma.

Lemma 2 [33]: For any matrix satisfying $\mathbf{W} = \mathbf{w}\mathbf{w}^H$, the following conditions equivalently hold:

$$\begin{bmatrix} \mathbf{M}_1 & \mathbf{W} & \mathbf{w} \\ \mathbf{W}^H & \mathbf{M}_2 & \mathbf{w} \\ \mathbf{w}^H & \mathbf{w}^H & \mathbf{1} \end{bmatrix} \succeq 0, \tag{28}$$

$$\mathrm{Tr}\left(\mathbf{w}\mathbf{w}^H - \mathbf{M}_1\right) \geq 0, \tag{29}$$

$$\begin{aligned}
\sum_{k=1}^{K} f_k\left(\mathbf{V}_k, \mathbf{Q}_k, \mathbf{U}_k, \mathbf{Z}_k\right) &= -\sum_{k=1}^{K} \mathrm{Tr}\left(\mathbf{Z}_k \mathbf{E}_k\right) \\
&= -\sum_{k=1}^{K} \mathrm{Tr}\left\{\mathbf{Z}_k \left[\mathbf{U}_k^H \left(\mathbf{I} + \sum_{k' \neq k}^{K} \overline{\mathbf{H}}_k \mathbf{V}_{k'} \mathbf{V}_{k'}^H \overline{\mathbf{H}}_k^H\right) \mathbf{U}_k + \left(\mathbf{I} - \mathbf{U}_k^H \overline{\mathbf{H}}_k \mathbf{V}_k\right) \left(\mathbf{I} - \mathbf{U}_k^H \overline{\mathbf{H}}_k \mathbf{V}_k\right)^H\right]\right\} \\
&= -\sum_{k=1}^{K} \left\{\mathrm{Tr}\left[\mathbf{Z}_k \mathbf{U}_k^H \left(\mathbf{I} + \sum_{k' \neq k}^{K} \overline{\mathbf{H}}_k \mathbf{V}_{k'} \mathbf{V}_{k'}^H \overline{\mathbf{H}}_k^H\right) \mathbf{U}_k\right] - \mathrm{Tr}\left[\mathbf{Z}_k \left(\mathbf{I} - \mathbf{U}_k^H \overline{\mathbf{H}}_k \mathbf{V}_k\right) \left(\mathbf{I} - \mathbf{U}_k^H \overline{\mathbf{H}}_k \mathbf{V}_k\right)^H\right]\right\} \\
&= \sum_{k=1}^{K} \mathrm{Tr}\left(\mathbf{Z}_k \mathbf{U}_k^H \overline{\mathbf{H}}_k \mathbf{V}_k\right) + \sum_{k=1}^{K} \mathrm{Tr}\left(\mathbf{Z}_k \mathbf{V}_k^H \overline{\mathbf{H}}_k^H \mathbf{U}_k\right) - \sum_{k=1}^{K} \mathrm{Tr}\left(\mathbf{Z}_k \mathbf{U}_k^H \left(\sum_{k'=1}^{K} \overline{\mathbf{H}}_{k'} \mathbf{V}_{k'} \mathbf{V}_{k'}^H \overline{\mathbf{H}}_{k'}^H\right) \mathbf{U}_k\right) \\
&= 2\sum_{k=1}^{K} \Re\left\{\mathrm{Tr}\left(\mathbf{Z}_k \mathbf{U}_k^H \overline{\mathbf{H}}_k \mathbf{V}_k\right)\right\} - \sum_{k=1}^{K} \mathrm{Tr}\left(\mathbf{V}_k^H \sum_{k'=1}^{K} \left(\overline{\mathbf{H}}_{k'}^H \mathbf{U}_{k'} \mathbf{Z}_{k'} \mathbf{U}_{k'}^H \overline{\mathbf{H}}_{k'}\right) \mathbf{V}_k\right)
\end{aligned} \tag{13}$$

$$\sum_{k=1}^{K} \mathrm{Tr}\left(\mathbf{V}_k^H \mathbf{A} \mathbf{V}_k\right) = \sum_{k=1}^{K} \mathrm{Tr}\left(\mathbf{Q}_k^H \mathbf{H}_k^H \mathbf{U}_k \mathbf{Z}_k \mathbf{U}_k^H \mathbf{H}_k \mathbf{Q}_k \mathbf{F} \sum_{k'=1}^{K} \mathbf{V}_{k'} \mathbf{V}_{k'}^H\right) / \sigma_k^2 \tag{19}$$

$$\sum_{k=1}^{K} 2\Re\left\{\mathrm{Tr}\left(\mathbf{B}_k \mathbf{V}_k\right)\right\} = \sum_{k=1}^{K} 2\Re\left\{\mathrm{Tr}\left(\mathbf{Z}_k \mathbf{U}_k^H \mathbf{H}_k \mathbf{Q}_k \mathbf{F} \mathbf{V}_k\right)\right\} / \sigma_k \tag{20}$$

Authorized licensed use limited to: Nanjing University. Downloaded on March 10,2026 at 07:06:34 UTC from IEEE Xplore. Restrictions apply.

where $\mathbf{M}_1$, $\mathbf{M}_2 \in \mathbb{H}^{N\times N}$ are slack variables and $\mathbb{H}^{N\times N}$ represents an $N \times N$ dimensional Hermitian matrix.

Based on *Lemma 2*, Problem (27) can be rewritten as

$$\underset{\mathbf{q}_k,\widetilde{\mathbf{q}}_k}{\text{minimize}} \sum_{k=1}^{K} \left(\mathbf{q}_k^H \mathbf{G}_k \mathbf{q}_k/\sigma_k^2 - 2\Re\left\{\mathbf{q}_k^H \mathbf{p}_k\right\}/\sigma_k\right) \tag{30a}$$

$$\text{s.t. } \operatorname{diag}\left(\boldsymbol{\Theta}_k + \widetilde{\boldsymbol{\Theta}}_k\right) = \mathbf{1}_{LM}, \tag{30b}$$

$$\begin{bmatrix} \mathbf{M}_1 & \mathbf{Q}_k & \mathbf{q}_k \\ \mathbf{Q}_k^H & \mathbf{M}_2 & \mathbf{q}_k \\ \mathbf{q}_k^H & \mathbf{q}_k^H & 1 \end{bmatrix} \succeq 0, \tag{30c}$$

$$\operatorname{Tr}\left(\mathbf{q}_k \mathbf{q}_k^H\right) \geq \operatorname{Tr}\left(\mathbf{M}_1\right), \tag{30d}$$

$$\begin{bmatrix} \widetilde{\mathbf{M}}_1 & \widetilde{\mathbf{Q}}_k & \widetilde{\mathbf{q}}_k \\ \widetilde{\mathbf{Q}}_k^H & \widetilde{\mathbf{M}}_2 & \widetilde{\mathbf{q}}_k \\ \widetilde{\mathbf{q}}_k^H & \widetilde{\mathbf{q}}_k^H & 1 \end{bmatrix} \succeq 0, \tag{30e}$$

$$\operatorname{Tr}\left(\widetilde{\mathbf{q}}_k \widetilde{\mathbf{q}}_k^H\right) \geq \operatorname{Tr}\left(\widetilde{\mathbf{M}}_1\right), \tag{30f}$$

where $\mathbf{M}_1, \mathbf{M}_2, \widetilde{\mathbf{M}}_1, \widetilde{\mathbf{M}}_2 \in \mathbb{H}^{N\times N}$ are slack variables.

Up to this point, the constraints (30d) and (30f) are still non-convex because they are in the form of "convex function $\geq$ affine function". Hence, we employ the CCCP method and replace the left-hand-side (LHS) functions of (30d) and (30f) with their first-order approximations as the surrogate functions. Due to the convexity of both functions, we have

$$\begin{aligned} \chi^n\left(\mathbf{q}_k\right) &\triangleq 2\Re\left\{\left(\mathbf{q}_k^n\right)^H \mathbf{q}_k\right\} - \left(\mathbf{q}_k^n\right)^H \mathbf{q}_k^n \\ &\leqslant \quad \text{LHS of (30d)}, \end{aligned} \tag{31}$$

$$\begin{aligned} \widetilde{\chi}^n\left(\widetilde{\mathbf{q}}_k\right) &\triangleq 2\Re\left\{\left(\widetilde{\mathbf{q}}_k^n\right)^H \widetilde{\mathbf{q}}_k\right\} - \left(\widetilde{\mathbf{q}}_k^n\right)^H \widetilde{\mathbf{q}}_k^n \\ &\leqslant \quad \text{LHS of (30f)}, \end{aligned} \tag{32}$$

where $\mathbf{q}_k^n$ and $\widetilde{\mathbf{q}}_k^n$ denote the solution of $\mathbf{q}_k$ and $\widetilde{\mathbf{q}}_k$ obtained in the nth iteration of our algorithm. The function $\chi\left(\mathbf{q}_k\right)$ and $\widetilde{\chi}^n\left(\widetilde{\mathbf{q}}_k\right)$ are the first-order approximations of the LHS functions of (30d) and (30f), respectively. Therefore, by substituting $\chi\left(\mathbf{q}_k\right)$ and $\widetilde{\chi}^n\left(\widetilde{\mathbf{q}}_k\right)$ for the LHS functions of (30d) and (30f), we can approximate Problem (30) by the following problem in the $(n+1)$th iteration:

$$\underset{\mathbf{q}_k,\widetilde{\mathbf{q}}_k}{\text{minimize}} \sum_{k=1}^{K} \left(\mathbf{q}_k^H \mathbf{G}_k \mathbf{q}_k/\sigma_k^2 - 2\Re\left\{\mathbf{q}_k^H \mathbf{p}_k\right\}/\sigma_k\right) \tag{33a}$$

$$\text{s.t. } \operatorname{diag}\left(\boldsymbol{\Theta}_k + \widetilde{\boldsymbol{\Theta}}_k\right) = \mathbf{1}_{LM}, \tag{33b}$$

$$\begin{bmatrix} \mathbf{M}_1 & \mathbf{Q}_k & \mathbf{q}_k \\ \mathbf{Q}_k^H & \mathbf{M}_2 & \mathbf{q}_k \\ \mathbf{q}_k^H & \mathbf{q}_k^H & 1 \end{bmatrix} \succeq 0, \tag{33c}$$

$$\chi^n\left(\mathbf{q}_k\right) \geq \operatorname{Tr}\left(\mathbf{M}_1\right), \tag{33d}$$

$$\begin{bmatrix} \widetilde{\mathbf{M}}_1 & \widetilde{\mathbf{Q}}_k & \widetilde{\mathbf{q}}_k \\ \widetilde{\mathbf{Q}}_k^H & \widetilde{\mathbf{M}}_2 & \widetilde{\mathbf{q}}_k \\ \widetilde{\mathbf{q}}_k^H & \widetilde{\mathbf{q}}_k^H & 1 \end{bmatrix} \succeq 0, \tag{33e}$$

$$\widetilde{\chi}^n\left(\widetilde{\mathbf{q}}_k\right) \geq \operatorname{Tr}\left(\widetilde{\mathbf{M}}_1\right), \tag{33f}$$

which can be solved by convex optimization packages such as CVX. After solving Problem (33) and obtaining the optimal $\mathbf{q}_k^\star$, we can get the optimal solution of $\mathbf{Q}_k^\star$ by $\mathbf{Q}_k^\star = \operatorname{diag}\left(\mathbf{q}_k^\star\right)$.

C. Overall Algorithm Description and Complexity Analysis

We summarize the proposed BCD algorithm in **Algorithm 1**, which solves the downlink sum-rate maximization problem (6).

Algorithm 1 BCD Algorithm for Problem (6)

1: Initialize maximum outer and inner iteration numbers, namely $I_{\max}$ and $N_{\max}$, as well as threshold ϵ_{Rate};
2: Initialize a feasible point $\left\{\mathbf{V}_k^0, \mathbf{Q}_k^0\right\}$;
3: **while** $i \leq I_{\max}$ **and** $\left|\sum_{k=1}^K f_k^{i+1} - \sum_{k=1}^K f_k^i\right| \geq \epsilon_{\text{Rate}}$ **do**
4: Calculate $\mathbf{U}_k^i$ by (11);
5: Calculate $\mathbf{Z}_k^i$ by (12);
6: Calculate $\mathbf{V}_k^{i\,\star}$ by (16);
7: **while** $n \leq N_{\max}$ **and** $\left|\sum_{k=1}^K f_k^{n+1} - \sum_{k=1}^K f_k^n\right| \geq \epsilon_{\text{Rate}}$ **do**
8: Calculate $\mathbf{q}_k^n$, $\mathbf{p}_k^n$, $\mathbf{G}_k^n$;
9: Calculate $\mathbf{q}_k^{n\star}$ by solving Problem (33);
10: $n = n + 1$.
11: **end while**
12: Set $\mathbf{Q}_k^{i\,\star} = \operatorname{diag}\left(\mathbf{q}_k^{i\,\star}\right)$;
13: $i = i + 1$.
14: **end while**
15: **output** $\{\mathbf{V}_k^\star, \mathbf{Q}_k^\star\}$.

We first optimize the objective function of Problem (6) by utilizing WMMSE and introducing auxiliary variables $\mathbf{U}_k$ and $\mathbf{Z}_k$. Based on that, the complex non-convex problem can be transformed into a problem that can be solved in an iterative manner. Next, we employ the lower-complexity Lagrangian dual method to optimize the beamforming matrix $\mathbf{V}_k$ and obtain the optimal beamforming matrix $\mathbf{V}_k$ through a bisection search algorithm. Finally, for the optimization of the equivalent TRC matrix $\mathbf{Q}_k$ in the case of multiple STAR-RISs, we first relax the non-convex constraints by analyzing the relationship between the users and the STAR-RISs, and then optimize the TRC matrix $\mathbf{Q}_k$ through the CCCP algorithm to obtain the optimal solution.

The complexity of **Algorithm 1** can be analyzed as follows. According to [31], in **Step 4** of **Algorithm 1**, the complexity of computing the decoding matrix $\mathbf{U}_k$ is $\mathcal{O}\left(KN_{\text{U}}^3\right)$. In **Step 5**, the complexity of calculating the auxiliary matrix $\mathbf{Z}_k$ is given by $\mathcal{O}\left(Kd^3\right)$, where d denotes the corresponding number of data streams (which is set as N_{U} in our simulations). In **Step 6**, we have to calculate the beamforming matrices $\mathbf{V}_k$. We assume $N_{\text{B}} \geq N_{\text{U}} \geq d$ (and this is how we set in simulations). Hence, the complexity of computing the auxiliary matrices $\mathbf{A}_k$ is given by $\mathcal{O}\left(KN_{\text{B}}^2 d\right)$. The complexity of calculating $\mathbf{V}_k$ in (16) is given by $\mathcal{O}\left(KN_{\text{B}}^3\right)$. The number of iterations required for binary search can be represented as $\log_2\left(\frac{\lambda_{\text{u}}-\lambda_{\text{l}}}{\varepsilon}\right)$, where λ_{u} and λ_{l} is the upper and lower bound of λ in binary search, and ε is the threshold for binary search to terminate. Hence, the overall complexity of calculating the beamforming matrices $\mathbf{V}_k$ is given by $\mathcal{O}\left(\log_2\left(\frac{\lambda_{\text{u}}-\lambda_{\text{l}}}{\varepsilon}\right) KN_{\text{B}}^3\right)$.

Then, for the CCCP method to update $\mathbf{Q}_k$, according to [33], in each iteration, the complexity of solving (33) is

Authorized licensed use limited to: Nanjing University. Downloaded on March 10,2026 at 07:06:34 UTC from IEEE Xplore. Restrictions apply.

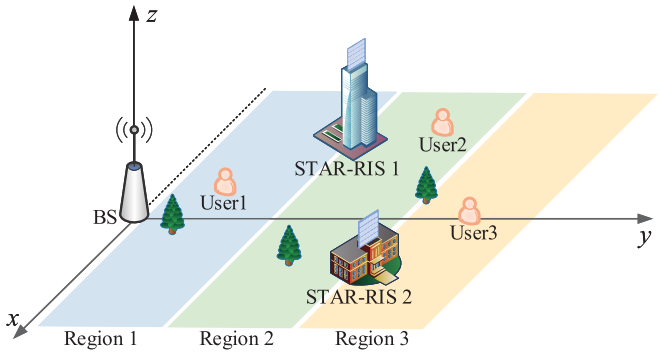

Fig. 3. The simulation scenario of the multi-STAR-RIS-assisted MIMO network.

$\mathcal{O}\left((LM)^3\right)$. Thus, the total complexity for calculating $\mathbf{Q}_k$ is $\mathcal{O}\left(N_{\text{ite}}(LM)^3\right)$, where N_{ite} denotes the iteration number of the CCCP method. According to the above analysis, the overall complexity of **Algorithm 1** can be estimated by

$$\mathcal{O}\left(I_{\text{ite}} \cdot \max\left\{\log_2\left(\frac{\lambda_{\text{u}}-\lambda_{\text{l}}}{\varepsilon}\right) K N_{\text{B}}^3, N_{\text{ite}}(LM)^3\right\}\right), \tag{34}$$

where I_{ite} denotes the number of iterations for the outer iteration in **Algorithm 1**.

V. Performance Evaluation

In this section, numerical results are presented to demonstrate the effectiveness of the proposed method for multi-STAR-RIS-assisted MIMO communication systems. We investigate the impact of different operating schemes, transmit power, and the number of elements on the sum rate of the system. We also compare the TRCs of each STAR-RIS/RIS element under different schemes and analyze the impact of the chosen scheme on the overall system performance in terms of the sum rate.

A. Simulation Setup

Fig. 3 illustrates the considered simulation scenario, where the BS and the STAR-RISs are located at $(0\text{m}, 0\text{m}, 20\text{m})$, $(-20\text{m}, 20\text{m}, 25\text{m})$ and $(20\text{m}, 40\text{m}, 15\text{m})$, respectively. K users are randomly allocated to the three regions separated by the STAR-RISs.

All channels are assumed to follow the narrow band quasi-static fading model [10]. Thus, the channel from the BS to the lth STAR-RIS and the channel from the lth STAR-RIS to the kth user can be modeled as Rician fading channels as follows:

$$\mathbf{F}_l = \sqrt{\frac{\rho_0}{d_{\text{BR},l}^{\alpha_{\text{BR}}}}}\left(\sqrt{\frac{K_{\text{BR}}}{K_{\text{BR}}+1}}\mathbf{F}_l^{\text{LoS}} + \sqrt{\frac{1}{K_{\text{BR}}+1}}\mathbf{F}_l^{\text{NLoS}}\right), \tag{35}$$

$$\mathbf{H}_k^l = \sqrt{\frac{\rho_0}{d_{\text{RU},k}^{\alpha_{\text{RU}}}}}\left(\sqrt{\frac{K_{\text{RU}}}{K_{\text{RU}}+1}}\mathbf{H}_k^{l,\text{LoS}} + \sqrt{\frac{1}{K_{\text{RU}}+1}}\mathbf{H}_k^{l,\text{NLoS}}\right), \tag{36}$$

where $d_{\text{BR},l}$ and $d_{\text{RU},k}$ respectively denote the distance between the BS and the lth STAR-RIS and between the lth STAR-RIS and the kth user, α_{BR} and α_{RU} respectively represent the corresponding path loss exponents, K_{BR} and K_{RU} respectively denote the Rician factors, ρ_0 represents the pathloss at a reference distance of 1 meter, $\mathbf{F}^{\text{LoS}}$ and $\mathbf{H}_k^{l,\text{LoS}}$ are the deterministic line-of-sight (LoS) components, and $\mathbf{F}^{\text{NLoS}}$ and $\mathbf{H}_k^{l,\text{NLoS}}$ are the random non-line-of-sight (NLoS) components modeled as Rayleigh fading.

TABLE I
Default Simulation Parameter

Symbols	Physical Meaning	Values
N_{B}	The number of BS antennas	4
N_{U}	The number of antennas at each user	2
K	The number of users	3
L	The number of STAR-RISs	2
M	The number of element at each STAR-RIS/RIS	32
α_{BR}	Pathloss exponent for the BS-STAR-RIS channels	2.2
α_{RU}	Pathloss exponent for the STAR-RIS-user channels	2.2
K_{BR}	Rician factor for the BS-STAR-RIS channels	3
K_{BU}	Rician factor for the STAR-RIS-user channels	3
ρ_0	Pathloss at 1 meter	-30 dB
σ_k^2	User noise power	-90 dBm
σ_{CEE}^2	The channel estimation error variance	0.2/0.4/0.6
$I_{\max}$	Max number of outer iterations in **Algorithm 1**	40
$N_{\max}$	Max number of inner iterations in **Algorithm 1**	25

It is assumed that uniform square planar arrays (USPAs) are equipped at the BS and the STAR-RIS [34]. Then, the LoS components can be modeled as:

$$\mathbf{F}_l^{\text{LoS}} = \mathbf{a}_{\text{RIS}}\left(\theta_{\text{AoA}}^{\text{a}}, \theta_{\text{AoA}}^{\text{e}}\right)\mathbf{a}_{\text{BS}}^H\left(\omega_{\text{AoD}}^{\text{a}}, \omega_{\text{AoD}}^{\text{e}}\right), \tag{37}$$

$$\mathbf{H}_k^{l,\text{LoS}} = \mathbf{a}_{\text{User}}\left(\varphi_{\text{AoA}}^{\text{a}}, \varphi_{\text{AoA}}^{\text{e}}\right)\mathbf{a}_{\text{RIS}}^H\left(\psi_{\text{AoD}}^{\text{a}}, \psi_{\text{AoD}}^{\text{e}}\right). \tag{38}$$

Here, $\omega_{\text{AoD}}^{\text{a}}, \omega_{\text{AoD}}^{\text{e}}$ are the azimuth and elevation angles of departure (AoDs) at the STAR-RIS, respectively. $\psi_{\text{AoD}}^{\text{a}}, \psi_{\text{AoD}}^{\text{e}}$ are the azimuth and elevation AoDs at the user, respectively. $\theta_{\text{AoA}}^{\text{a}}$ and $\theta_{\text{AoA}}^{\text{e}}$ are the azimuth and elevation angles of arrival (AoAs) at the STAR-RIS from BS, respectively. $\varphi_{\text{AoA}}^{\text{a}}$ and $\varphi_{\text{AoA}}^{\text{e}}$ are the azimuth and elevation AoAs at the user from the STAR-RIS, respectively. The array response vector $\mathbf{a}_{\text{P}}\left(\varpi^{\text{a}}, \varpi^{\text{e}}\right), \text{P} \in \{\text{RIS}, \text{BS}, \text{User}\}$ is given by

$$\mathbf{a}_{\text{P}}\left(\varpi^{\text{a}}, \varpi^{\text{e}}\right) = \Big[1, \cdots, e^{j2\pi\frac{s}{\nu}\left(x\sin\varpi^{\text{a}}\sin\varpi^{\text{e}} + y\cos\varpi^{\text{e}}\right)}, e^{j2\pi\frac{s}{\nu}\left(\left(\sqrt{X}-1\right)\sin\varpi^{\text{a}}\sin\varpi^{\text{e}} + \left(\sqrt{X}-1\right)\cos\varpi^{\text{e}}\right)}\Big]^{\mathsf{T}}, \tag{39}$$

where ϖ^{a} and ϖ^{e} denote the azimuth and elevation AoAs or AoDs. $x = \lfloor (m-1)/\sqrt{M} \rfloor$ and $y = (m-1)\text{mod}\sqrt{M}$. Moreover, s denotes the element/antenna spacing and ν denotes the carrier wavelength. For simplicity, we set $s/\nu = 1/2$. The default simulation parameters are presented in Table I [10].

For comparison, the following benchmark schemes are considered:

1) *Multiple STAR-RISs with TS (MSRTS) Scheme*: In this case, all the elements of the STAR-RISs can only operate in one mode within a time slot, i.e, either reflecting signals or transmitting signals. For simplicity, we neglect the synchronization errors between different STAR-RISs

Authorized licensed use limited to: Nanjing University. Downloaded on March 10,2026 at 07:06:34 UTC from IEEE Xplore. Restrictions apply.

and assume that all STAR-RISs within each time slot operate in the same mode.

2) *Multiple STAR-RISs with SDR (MSR-SDR) Scheme*: In this scheme, we still consider the same system setting as our proposed scheme, but we use the semi-definite relaxation (SDR) algorithm in [10] with Gaussian randomization to optimize the TRC matrices in Problem (30) and compare its performance with our proposed scheme.
3) *Multiple STAR-RISs with MS (MSRMS) Scheme*: In this case, all elements of each STAR-RIS are divided into two states. One state contains M^{t} elements that operate in the transmission state while the other state contains M^{r} elements operating in the reflection state, where $M^{\mathrm{t}} + M^{\mathrm{r}} = M$. The STAR-RIS TRC matrices is given by $\mathbf{\Phi}_{\xi}^{l,\mathrm{MS}} = \mathrm{diag}\left(\sqrt{\beta_{1,l}^{\xi}}e^{j\phi_{1,l}^{\xi}}, \cdots, \sqrt{\beta_{M,l}^{\xi}}e^{j\phi_{M,l}^{\xi}}\right) \in \mathbb{C}^{M\times M}$ where $\beta_{m,l}^{\xi} \in \{0,1\}$, $\phi_{m,l}^{\xi} \in [0, 2\pi)$ and $\beta_{m,l}^{\mathrm{t}} + \beta_{m,l}^{\mathrm{r}} = 1$.
4) *Multiple STAR-RISs with Equal ES (MSREES) Scheme*: In this case, each element of each STAR-RIS has the same transmitting and reflecting coefficients, i.e., $\beta_{m,l}^{\mathrm{t}} = \beta_{m,l}^{\mathrm{r}} = 0.5$. For this scheme, we mainly focus on the phases $\phi_{m,l}^{\mathrm{t}}, \phi_{m,l}^{\mathrm{r}}$ of each STAR-RIS element to maximize the sum rate for all users.
5) *Conventional Multiple RISs (CMR) Scheme*: We replace each STAR-RIS with two adjacent RISs. Since each STAR-RIS operates in the ES scheme in our proposed scheme, each element can transmit and reflect signals simultaneously. To ensure fairness in comparison between multiple STAR-RISs and multiple RISs, we assume that both adjacent RISs have $M/2$ elements, with one only reflecting signals and the other only transmitting signals.
6) *Single STAR-RIS (SSR) Scheme*: In this case, we remove the STAR-RIS located at $(20\mathrm{m}, 40\mathrm{m}, 15\mathrm{m})$ and simplify the situation to only one STAR-RIS. To ensure fairness in comparison, we set the number of elements in the remaining STAR-RIS to $2M$.
7) *Conventional Single RIS (CSR) Scheme*: In this case, we remove the STAR-RIS located at $(20\mathrm{m}, 40\mathrm{m}, 15\mathrm{m})$ and replace the remaining STAR-RIS with two adjacent RISs. Similar to the CMR scheme, we assume that both adjacent RISs have M elements, with one only reflecting signals and the other only transmitting signals.

B. Convergence Analysis

Fig. 4 illustrates the impact of different number of BS transmit antennas N_{B}, number of receive antennas at each user N_{U}, and number of elements at each STAR-RIS M on the convergence performance of the proposed scheme. In this simulation, $P_{\max}$ is set to 30 dBm, the maximum number of inner iterations $N_{\max}$ is set to 25, and the maximum number of outer iterations $I_{\max}$ is set to 40. The x-axis in Fig. 4 represents the outer iteration index.

As can be seen in Fig. 4, when we increase N_{B}, N_{U}, and M, the sum rate of all users is improved. This is because increasing the number of transmit and receive antennas at the BS and each user allows more spatial multiplexing gain to be achieved, and more data streams can be transmitted. At the same time, increasing the number of elements M at each STAR-RIS/RIS enables more degrees-of-freedom for controlling the channel, which also improves the data rates in the system. By doubling the number of STAR-RIS elements M, the user sum rate improvement is more pronounced when N_{B} and N_{U} are large. For example, when $N_{\mathrm{B}} = 12$ and $N_{\mathrm{U}} = 8$, the sum rate increases about 2 bits/s/Hz, while the sum rate increases only about 0.6 bits/s/Hz when $N_{\mathrm{B}} = 4$ and $N_{\mathrm{U}} = 4$.

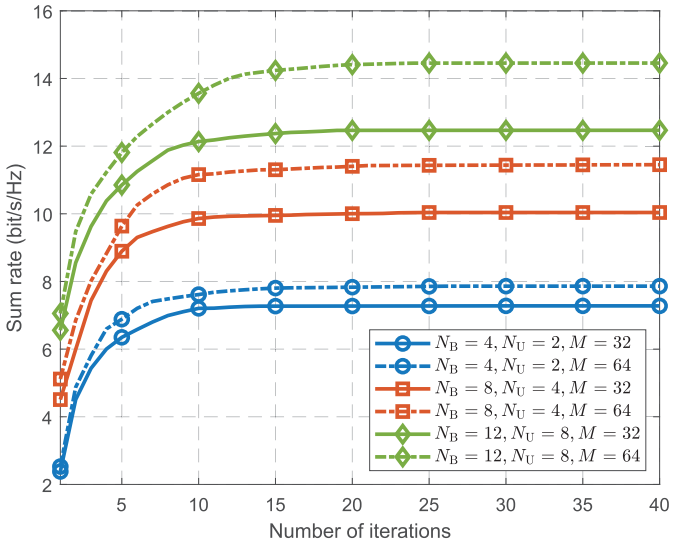

Fig. 4. Convergence analysis of proposed scheme for various N_{B}, N_{U}, and M where $P_{\max} = 30$ dBm.

C. Impact of Imperfect Channel State Information

In this subsection, we consider the impact of imperfect channel state information. We set the number of elements for each STAR-RIS as 32, the maximum transmit power of the BS as 30 dBm, the number of transmit antennas for the BS as four, and the number of receiving antennas for the user terminal as two.

We adopt the channel estimation model from [35], introducing channel estimation error matrices $\widetilde{\mathbf{F}}$ and $\widetilde{\mathbf{H}}_k$ into the channels from the BS to the STAR-RIS $\mathbf{F}$ and from the STAR-RIS to the kth user $\mathbf{H}_k$, where $\widetilde{\mathbf{F}}$ and $\widetilde{\mathbf{H}}_k$ are matrices whose elements follow i.i.d. complex normal distributions with zero mean and variance σ_{CEE}^2.

Fig. 5 presents the performance of the proposed scheme under different σ_{CEE}^2. Clearly, as σ_{CEE}^2 increases, the performance of the proposed scheme gradually becomes worse. This is because the inaccuracies in channel estimation prevent precise BS beamforming and TRC matrices optimization, resulting in an overall decrease in user communication rates. Considering the relatively large number of channels in the multi-STAR-RIS system, channel estimation errors will have a more pronounced impact in real systems.

D. Comparison With Benchmark Schemes

We set the number of elements for each STAR-RIS as 32, the maximum transmit power of the BS as 30 dBm, the number of transmit antennas for the BS as four, and the number of receiving antennas for the user terminal as two.

Authorized licensed use limited to: Nanjing University. Downloaded on March 10,2026 at 07:06:34 UTC from IEEE Xplore. Restrictions apply.

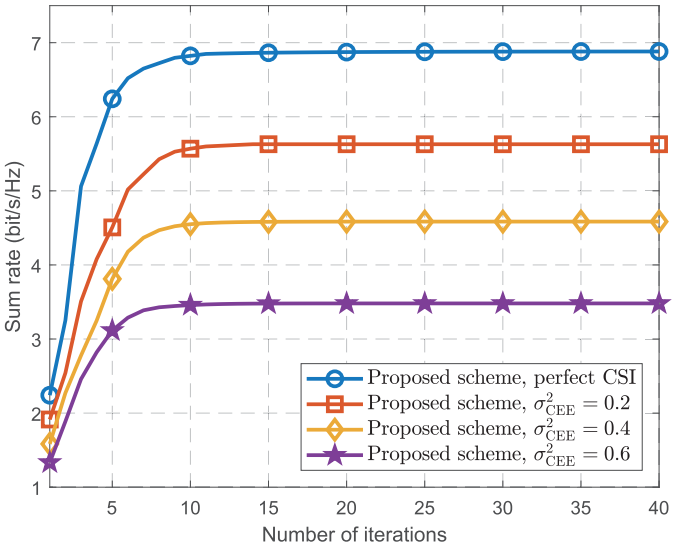

Fig. 5. User sum rate of proposed scheme under different channel estimation error variance σ^2_{CEE}.

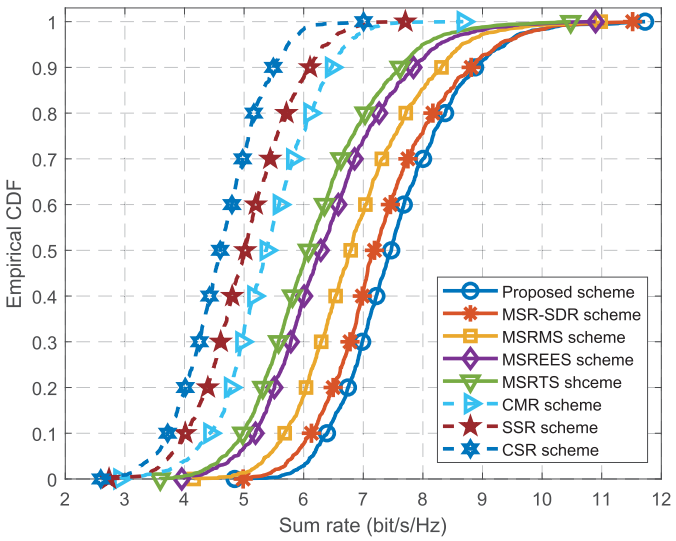

Fig. 6. The empirical CDF of sum rate of all schemes where $N_{\mathrm{B}} = 4, N_{\mathrm{U}} = 2, M = 32$ and $P_{\max} = 30$ dBm.

To validate the performance of different schemes, the simulations are conducted as follows: We randomly place users within each region and evaluate the performance of all schemes at each user locations. We perform $1,000$ user-location simulation runs for each scheme to observe their statistical performance. Fig. 6 presents the empirical CDF graph based on the simulation results of these schemes. From Fig. 6, it can be observed that our proposed scheme outperforms other schemes.

The performance of the MSR-SDP scheme, MSRMS scheme and the MSREES scheme are slightly inferior to our proposed scheme. This can be attributed to the fact that in the MSR-SDP scheme, Problem (30) is solved through SDR with Gaussian randomization, and the solution of this scheme is not as good as our proposed scheme. In the MSRMS scheme, each element of the STAR-RIS is limited to operating in either the reflection or transmission state. In contrast, our proposed scheme enables flexible adjustment of the TRC for each element, resulting in better performance. In the MSREES, the fixed transmitting and reflecting coefficients limit its overall performance. The performance of the MSRTS scheme is slightly inferior than the MSREES scheme. The reason could be that, in the MSRTS scheme, each STAR-RIS operates in the same state within a time slot, leaving at least one user unserved in every time slot.

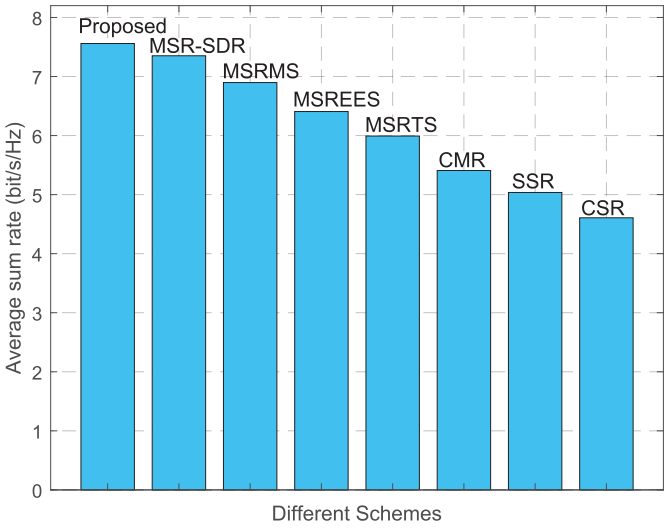

Fig. 7. Average sum rate comparison of different schemes based on empirical CDF results.

Furthermore, the performance of other schemes considered in the benchmarks is comparatively worse than that of our proposed scheme. The CMR scheme performs worse than the multi-STAR-RIS scheme when considering the overall service for all users, as the RIS can only serve users on one side. The CSR scheme and SSR scheme achieve poorer performance compared to multiple STAR-RIS/RIS case. This is because, by removing additional STAR-RISs/RISs, the average distance between the remaining STAR-RIS/RIS and the users increases. Therefore, the average signal quality degrades, even though we increase the number of elements at the remaining STAR-RIS/RIS.

Fig. 7 shows the bar chart of average rates for different schemes obtained from $1,000$ random simulations. In terms of performance, our proposed scheme achieves a 2.82%, 9.59%, 17.97%, and 26.14% improvement over the MSR-SDP scheme, the MSRMS scheme, the MSREES scheme, and the MSRTS scheme, respectively. Compared to the CMR scheme, our proposed scheme provides a 38.99% improvement, while compared to the SSR scheme and CSR scheme, it yields a 51.07% and 63.85% improvement, respectively. The reasons behind these observations are similar to the explanations provided for Fig. 6.

E. Impact of User Numbers

In order to verify the feasibility of the proposed model with different numbers of users, we perform a comparative study for the proposed scheme under different number of users. We set the number of elements for each STAR-RIS as 32, the maximum transmit power of the BS as 30 dBm, the number of transmit antennas for the BS as four, and the number of receiving antennas for the user terminal as two. The initial

Authorized licensed use limited to: Nanjing University. Downloaded on March 10,2026 at 07:06:34 UTC from IEEE Xplore. Restrictions apply.

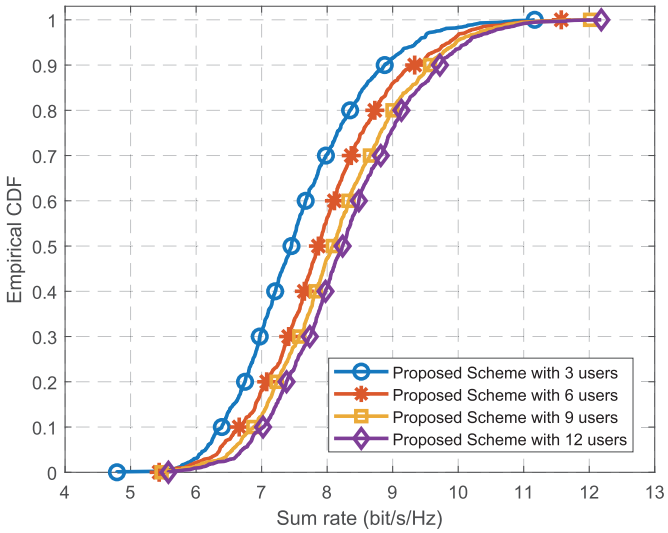

Fig. 8. The empirical CDF of sum rate of different numbers of users under the proposed scheme where $N_{\mathrm{B}} = 4, N_{\mathrm{U}} = 2, M = 32$ and $P_{\max} = 30$ dBm.

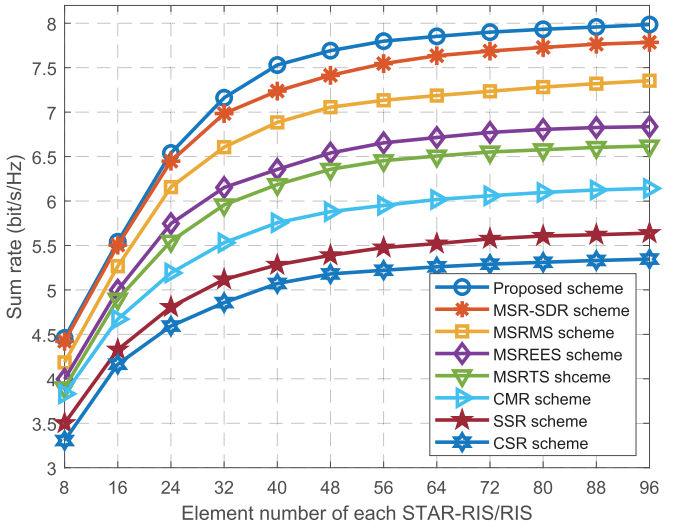

Fig. 10. The sum rate versus the number of elements at each STAR-RIS/RIS where $N_{\mathrm{B}} = 4, N_{\mathrm{U}} = 2$ and $P_{\max} = 30$ dBm.

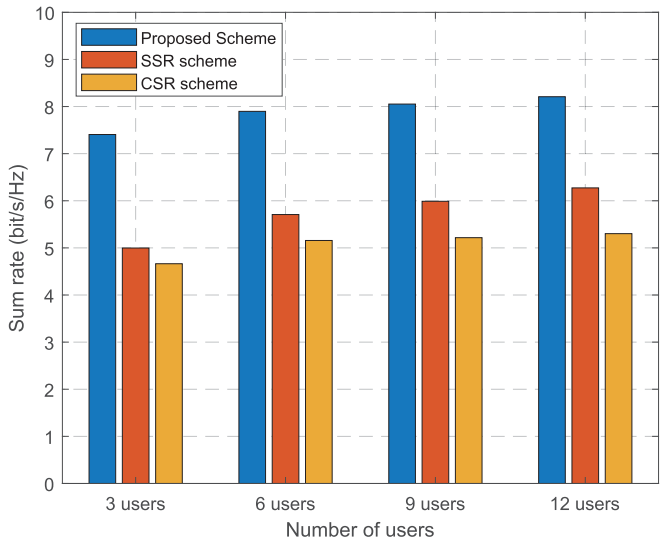

Fig. 9. Average sum rate comparison of different numbers of users based on empirical CDF results.

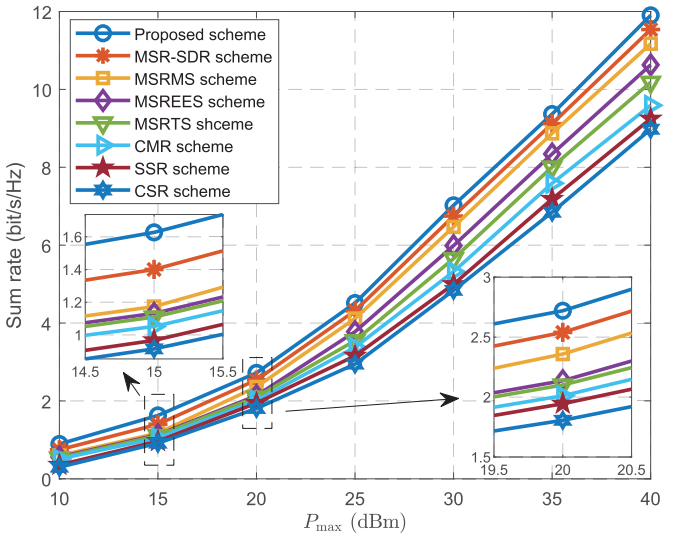

Fig. 11. The sum rate versus the max transmit power $P_{\max}$ where $N_{\mathrm{B}} = 4, N_{\mathrm{U}} = 2$ and $M = 32$.

number of users is 3, and then the number of users in each region increases by 1 until the total number of users in the entire system reaches 12.

As shown in Fig. 8, in the scenario where user locations are randomly distributed 1000 times, the proposed scheme still maintains good performance with 12 users. Compared to the case with 3 users, the average user sum rates increases by 5.13%, 7.90%, and 9.88% for 6, 9, and 12 users, respectively. Additionally, the improvements of average user sum rates from 3 users to 6 users, from 6 users to 9 users, and from 9 users to 12 users were 5.13%, 2.63%, and 1.83%, respectively. This is because as the number of users increases, the interference among them also increases, resulting in a relatively smaller overall increase in user sum rates.

We also consider the performance comparison of the proposed scheme, SSR scheme, and CSR scheme for different numbers of users. Fig. 9 provides a bar chart comparing the performance of the three schemes as the number of users varies. Clearly, the performance of multi-STAR-RIS remains superior to that of single STAR-RIS and single RIS. Moreover, it is observed that the average sum rate growth of the single RIS case is inferior to that of single STAR-RIS and multi-STAR-RIS cases as the number of users increases.

F. Impact of Element Number at Each STAR-RIS/RIS

Fig. 10 demonstrates the performance of different schemes under varying numbers of STAR-RIS/RIS elements. In the simulation, the maximum transmit power of the BS is set to 30 dBm, the number of transmit antennas in the BS is four, and the number of receive antennas is two, while only the number of elements at each STAR-RIS/RIS is changed.

As shown in Fig. 10, the performance of all schemes improves with the increase of the number of elements at each STAR-RIS/RIS. This is because with the increase in the number of elements, each STAR-RIS/RIS has more

Authorized licensed use limited to: Nanjing University. Downloaded on March 10,2026 at 07:06:34 UTC from IEEE Xplore. Restrictions apply.

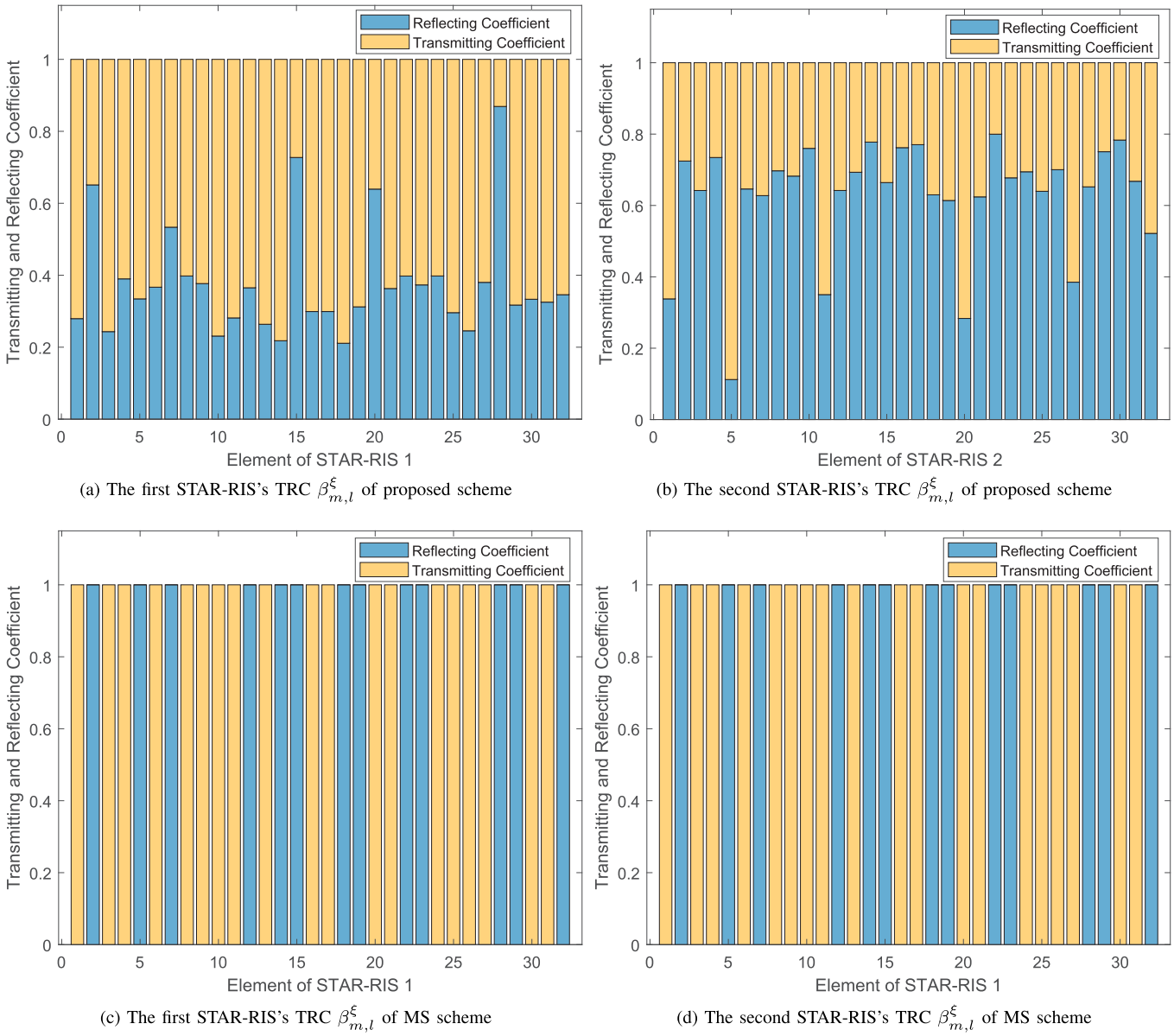

(a) The first STAR-RIS's TRC $\beta_{m,l}^{\xi}$ of proposed scheme

(b) The second STAR-RIS's TRC $\beta_{m,l}^{\xi}$ of proposed scheme

(c) The first STAR-RIS's TRC $\beta_{m,l}^{\xi}$ of MS scheme

(d) The second STAR-RIS's TRC $\beta_{m,l}^{\xi}$ of MS scheme

Fig. 12. TRC of different schemes.

degrees-of-freedom to optimize the TRC matrices or the phases to improve the communication quality for all users.

The growth trend of our proposed scheme is similar to that of MSR-SDP, MSRMS, MSREES, and MSRTS schemes, as all these schemes consider multi-STAR-RIS. After the number of elements increases from 32 to 96, the performance improvements of these five schemes are 11.50%, 11.47%, 11.32%, 11.13%, and 11.11%, respectively. In contrast, the performance growth of the CMR, SSR, and CSR schemes is relatively slower. After the number of elements increases from 32 to 96, the system performance improves by 10.93%, 10.18%, and 10.08%, respectively. The performance growth of the MSRMS scheme is mainly because as the number of elements at each STAR-RIS increases, more parameters in the TRC matrices can be optimized in the MSRMS scheme, which can improve the communication performance of the system. The MSRTS and MSREES schemes only optimize the transmitting and reflecting phase shifts $\phi_{m,l}^{\mathrm{t}}$ and $\phi_{m,l}^{\mathrm{r}}$ while keeping the coefficients $\beta_{m,l}^{\mathrm{t}}$ and $\beta_{m,l}^{\mathrm{r}}$ of each element of the STAR-RIS fixed, but a larger number of elements in each STAR-RIS still provides more degrees-of-freedom for optimizing the effective channel, thus improving the communication quality for the users.

G. Impact of the Max Transmit Power $P_{\max}$

Fig. 11 presents the performance of different schemes under various BS transmit power. In the simulations, the element number of each STAR-RIS/RIS is set to 32, the number of the BS transmit antennas is four, and the number of user receive antennas is two, with only the maximum transmit power of the BS being varied.

As seen from Fig. 11, with the increment of BS transmit power, all schemes achieve some improvement in performance. This is because as the transmit power of the BS increases,

Authorized licensed use limited to: Nanjing University. Downloaded on March 10,2026 at 07:06:34 UTC from IEEE Xplore. Restrictions apply.

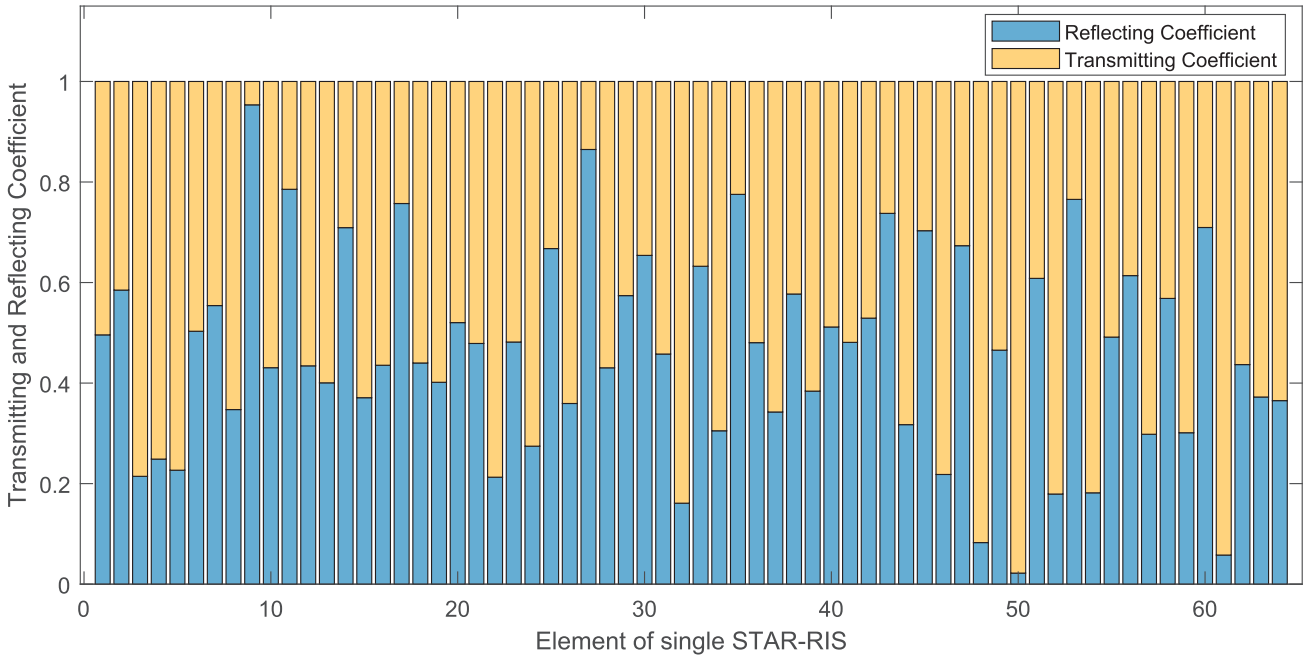

Fig. 13. The TRC β_m^{ξ} of single STAR-RIS scheme.

the signal-to-interference-plus-noise ratio (SINR) of the users improves, thereby enhancing the users' data rates.

When the transmit power is small, the difference in system performance among all schemes is small as shown in Fig. 11. However, as the transmit power increases, performance differences between the schemes gradually emerge. The main reason is that the user data rate is low when the transmit power is small. As the transmit power increases, the SINR improves, and optimizing the beamforming at BS as well as the TRC at the STAR-RIS/RIS can effectively enhance the communication quality for users. Therefore, the advantage of our proposed scheme compared to other schemes is more visible at high transmit power.

H. Analysis of TRCs

In this section, we compare the TRCs of different schemes related to STAR-RIS. In the simulations, the element number of each STAR-RIS/RIS is set to 32, the number of the BS transmit antennas is four, the number of user receive antennas is two, and the maximum transmit power of the BS is 30 dBm.

Fig. 12(a) and Fig. 12(b) show the TRCs of our proposed scheme for the first and the second STAR-RIS, respectively. In Fig. 12(a), we can observe that the transmitting coefficient is generally larger than the reflecting coefficient for the elements of the first STAR-RIS. However, the reverse is true for the elements of the second STAR-RIS as shown in Fig. 12(b), with the reflecting coefficient generally larger than the transmitting coefficient. This is because in our simulation setup, the BS is located on the far left, and the communication quality of users on the far right is often difficult to guarantee. Threfore, the first STAR-RIS, which is nearer to the BS, serves the users located on its transmission side by employing a higher transmission coefficient, while retaining a portion of its reflection coefficient to cater to users positioned on its reflection side. Conversely, the second STAR-RIS, which is farther to the BS, compensates for the lower reflection coefficient of the first STAR-RIS by employing a higher reflection coefficient, ensuring communication quality for users located on its reflection side, while also preserving some transmission coefficient to serve users on its transmission side.

Fig. 12(c) and Fig. 12(d) show the TRCs of the MS scheme. Fig. 12(c) represents the TRCs of the first STAR-RIS, while Fig. 12(d) represents the TRCs of the second STAR-RIS. Similar to our proposed scheme, in Fig. 12(c), more than half of the elements operate in the transmitting state, while in Fig. 12(d), more than half of the elements operate in the reflecting state. The reason for this aligns with the analysis presented in Fig. 12(a) and Fig. 12(b). Given the equal TRCs for elements of STAR-RISs in the MSREES scheme, i.e., $\beta^{\mathrm{t}} = \beta^{\mathrm{r}} = 0.5$, we omit the figure with the TRC results for the MSREES scheme.

Fig. 13 shows the TRCs of the SSR scheme, where only a single STAR-RIS is placed in the system. From Fig. 13, it can be seen that the transmitting coefficient of this STAR-RIS is higher than the reflecting coefficient for more than half of the elements. This is related to the simulation environment. Since there is only one user located in the reflecting region and two users in the transmitting region of the STAR-RIS, the TRC optimization is biased to the users in the transmitting region to ensure their communication quality.

VI. Conclusion

This paper investigates the downlink resource optimization for a MIMO communication system with multi-STAR-RIS assistance. Taking into account the beamforming of the BS and the coupling between multiple STAR-RISs, we address the problem of maximizing the sum rate subject to constraints of the transmit power of the BS and the coupling between

Authorized licensed use limited to: Nanjing University. Downloaded on March 10,2026 at 07:06:34 UTC from IEEE Xplore. Restrictions apply.

multiple STAR-RISs. To solve this problem, we use the BCD method to alternate between optimizing the active beamforming of the BS and the TRC matrices of the STAR-RISs. For the beamforming matrix design, we reformulate the problem using the WWMSE method and use the Lagrange duality method to obtain the optimal solution with reduced computational complexity. For the TRC matrix optimization, we introduce auxiliary variables to eliminate the coupling relationship and solve the problem by utilizing the CCCP method.

Our results show that the proposed scheme achieves a higher rate than other STAR-RIS working schemes, with superior performance under different element numbers of STAR-RIS and BS transmit power. Multiple STAR-RISs can serve more users and perform better than a single STAR-RIS. Moreover, the network performance assisted by STAR-RISs is generally superior to that assisted by conventional RISs.

For our future work, how to optimally deploy multiple STAR-RISs in networks needs to be explored, as the deployments of multi-STAR-RIS may affect the quality of both transmission and reflection channels. Additionally, imperfect channel state information and channel estimation in multi-STAR-RIS-assisted systems needs to be further investigated in the future research.

REFERENCES

[1] W. Saad, M. Bennis, and M. Chen, "A vision of 6G wireless systems: Applications, trends, technologies, and open research problems," *IEEE Netw.*, vol. 34, no. 3, pp. 134–142, May/Jun. 2019.

[2] Z. Zhang et al., "6G wireless networks: Vision, requirements, architecture, and key technologies," *IEEE Veh. Technol. Mag.*, vol. 14, no. 3, pp. 28–41, Sep. 2019.

[3] P. Yang, Y. Xiao, M. Xiao, and S. Li, "6G wireless communications: Vision and potential techniques," *IEEE Netw.*, vol. 33, no. 4, pp. 70–75, Jul. 2019.

[4] Q. Wu and R. Zhang, "Intelligent reflecting surface enhanced wireless network via joint active and passive beamforming," *IEEE Trans. Wireless Commun.*, vol. 18, no. 11, pp. 5394–5409, Nov. 2019.

[5] Y. Liu et al., "Reconfigurable intelligent surfaces: Principles and opportunities," *IEEE Commun. Surveys Tuts.*, vol. 23, no. 3, pp. 1546–1577, 3rd Quart., 2021.

[6] M. Di Renzo et al., "Smart radio environments empowered by reconfigurable intelligent surfaces: How it works, state of research, and the road ahead," *IEEE J. Sel. Areas Commun.*, vol. 38, no. 11, pp. 2450–2525, Nov. 2020.

[7] Y. Liu et al., "STAR: Simultaneous transmission and reflection for 360° coverage by intelligent surfaces," *IEEE Wireless Commun.*, vol. 28, no. 6, pp. 102–109, Dec. 2021.

[8] H. Zhang et al., "Intelligent omni-surfaces for full-dimensional wireless communications: Principles, technology, and implementation," *IEEE Commun. Mag.*, vol. 60, no. 2, pp. 39–45, Feb. 2022.

[9] J. Xu, Y. Liu, X. Mu, and O. A. Dobre, "STAR-RISs: Simultaneous transmitting and reflecting reconfigurable intelligent surfaces," *IEEE Commun. Lett.*, vol. 25, no. 9, pp. 3134–3138, Sep. 2021.

[10] X. Mu, Y. Liu, L. Guo, J. Lin, and R. Schober, "Simultaneously transmitting and reflecting (STAR) RIS aided wireless communications," *IEEE Trans. Wireless Commun.*, vol. 21, no. 5, pp. 3083–3098, May 2021.

[11] S. Hu, F. Rusek, and O. Edfors, "Beyond massive MIMO: The potential of data transmission with large intelligent surfaces," *IEEE Trans. Signal Process.*, vol. 66, no. 10, pp. 2746–2758, May 2018.

[12] C. Liaskos, S. Nie, A. Tsioliaridou, A. Pitsillides, S. Ioannidis, and I. Akyildiz, "A new wireless communication paradigm through software-controlled metasurfaces," *IEEE Commun. Mag.*, vol. 56, no. 9, pp. 162–169, Sep. 2018.

[13] H. Guo, Y.-C. Liang, J. Chen, and E. G. Larsson, "Weighted sum-rate maximization for reconfigurable intelligent surface aided wireless networks," *IEEE Trans. Wireless Commun.*, vol. 19, no. 5, pp. 3064–3076, May 2020.

[14] Z.-Q. He and X. Yuan, "Cascaded channel estimation for large intelligent metasurface assisted massive MIMO," *IEEE Wireless Commun. Lett.*, vol. 9, no. 2, pp. 210–214, Feb. 2019.

[15] J. Kim, J. Choi, J. Joung, and Y.-C. Liang, "Modified block coordinate descent method for intelligent reflecting surface-aided space-time line coded systems," *IEEE Wireless Commun. Lett.*, vol. 11, no. 9, pp. 1820–1824, Sep. 2022.

[16] D. Xu, X. Yu, Y. Sun, D. W. K. Ng, and R. Schober, "Resource allocation for secure IRS-assisted multiuser MISO systems," in *Proc. IEEE Globecom Workshops*, Waikoloa, HI, USA, Dec. 2019, pp. 1–6.

[17] J. Hu, Y.-C. Liang, Y. Pei, S. Sun, and R. Liu, "Reconfigurable intelligent surface based uplink MU-MIMO symbiotic radio system," *IEEE Trans. Wireless Commun.*, vol. 22, no. 1, pp. 423–438, Jan. 2023.

[18] M. Fu et al., "Reconfigurable intelligent surface empowered downlink non-orthogonal multiple access," *IEEE Trans. Commun.*, vol. 69, no. 6, pp. 3802–3817, Jun. 2021.

[19] S. Zeng, H. Zhang, B. Di, Z. Han, and L. Song, "Reconfigurable intelligent surface (RIS) assisted wireless coverage extension: RIS orientation and location optimization," *IEEE Commun. Lett.*, vol. 25, no. 1, pp. 269–273, Jan. 2021.

[20] L. Pang, J. Liu, Y. Zhang, X. Liu, Y. Chen, and A. Wang, "Deployment locations and beamforming optimization for multi-RIS in multi-BS networks," in *Proc. IEEE 98th Veh. Technol. Conf. (VTC-Fall)*, Hong Kong, Oct. 2023, pp. 1–6.

[21] J. Zhang, Z. Li, L. Shao, and W. Zhu, "Dynamical absorption manipulation in a graphene-based optically transparent and flexible metasurface," *Carbon*, vol. 176, pp. 374–382, May 2021.

[22] X. Wang, J. Ding, B. Zheng, S. An, G. Zhai, and H. Zhang, "Simultaneous realization of anomalous reflection and transmission at two frequencies using bi-functional metasurfaces," *Sci. Rep.*, vol. 8, no. 1, p. 1876, Jan. 2018.

[23] P. P. Perera, V. G. Warnasooriya, D. Kudathanthirige, and H. A. Suraweera, "Sum rate maximization in STAR-RIS assisted full-duplex communication systems," in *Proc. IEEE Int. Conf. Commun.*, Seoul, South Korea, May 2022, pp. 3281–3286.

[24] Q. Gao, Y. Liu, X. Mu, M. Jia, D. Li, and L. Hanzo, "Joint location and beamforming design for STAR-RIS assisted NOMA systems," *IEEE Trans. Commun.*, vol. 71, no. 4, pp. 2532–2546, Apr. 2023.

[25] C. Wu, X. Mu, Y. Liu, X. Gu, and X. Wang, "Resource allocation in STAR-RIS-aided networks: OMA and NOMA," *IEEE Trans. Wireless Commun.*, vol. 21, no. 9, pp. 7653–7667, Sep. 2022.

[26] R. Zhong, Y. Liu, X. Mu, Y. Chen, X. Wang, and L. Hanzo, "Hybrid reinforcement learning for STAR-RISs: A coupled phase-shift model based beamformer," *IEEE J. Sel. Areas Commun.*, vol. 40, no. 9, pp. 2556–2569, Sep. 2022.

[27] J. Zhao, Y. Zhu, X. Mu, K. Cai, Y. Liu, and L. Hanzo, "Simultaneously transmitting and reflecting reconfigurable intelligent surface (STAR-RIS) assisted UAV communications," *IEEE J. Sel. Areas Commun.*, vol. 40, no. 10, pp. 3041–3056, Oct. 2022.

[28] H. Niu, Z. Chu, F. Zhou, P. Xiao, and N. Al-Dhahir, "Weighted sum rate optimization for STAR-RIS-assisted MIMO system," *IEEE Trans. Veh. Technol.*, vol. 71, no. 2, pp. 2122–2127, Feb. 2022.

[29] Q. Shi, M. Razaviyayn, Z.-Q. Luo, and C. He, "An iteratively weighted MMSE approach to distributed sum-utility maximization for a MIMO interfering broadcast channel," *IEEE Trans. Signal Process.*, vol. 59, no. 9, pp. 4331–4340, Sep. 2011.

[30] M. Grant and S. Boyd. (2020). *CVX: MATLAB Software for Disciplined Convex Programming, Version 2.2*. [Online]. Available: http://cvxr.com/cvx

[31] C. Pan et al., "Multicell MIMO communications relying on intelligent reflecting surfaces," *IEEE Trans. Wireless Commun.*, vol. 19, no. 8, pp. 5218–5233, Aug. 2020.

[32] X. D. Zhang, *Matrix Analysis and Applications*. Beijing, China: Tsinghua Univ. Press, 2017.

[33] U. Rashid, H. D. Tuan, H. H. Kha, and H. H. Nguyen, "Joint optimization of source precoding and relay beamforming in wireless MIMO relay networks," *IEEE Trans. Commun.*, vol. 62, no. 2, pp. 488–499, Feb. 2014.

[34] H. Ren, X. Liu, C. Pan, Z. Peng, and J. Wang, "Performance analysis for RIS-aided secure massive MIMO systems with statistical CSI," *IEEE Wireless Commun. Lett.*, vol. 12, no. 1, pp. 124–128, Jan. 2023.

[35] L. Wei, C. Huang, G. C. Alexandropoulos, C. Yuen, Z. Zhang, and M. Debbah, "Channel estimation for RIS-empowered multi-user MISO wireless communications," *IEEE Trans. Commun.*, vol. 69, no. 6, pp. 4144–4157, Jun. 2021.

Authorized licensed use limited to: Nanjing University. Downloaded on March 10,2026 at 07:06:34 UTC from IEEE Xplore. Restrictions apply.

Qijie Liu received the B.S. degree from Zhejiang University of Technology, Hangzhou, China, in 2021, and the M.S. degree from the School of Electronic Science and Engineering, Nanjing University, Nanjing, China, in 2024. His research interests include reconfigurable intelligent surfaces and optimization in wireless communication networks.

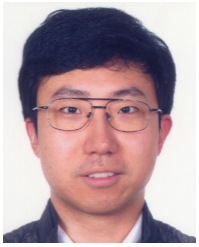

Jian Zhao (Senior Member, IEEE) received the B.S. degree from Nanjing University, Nanjing, China, the M.Sc. degree from Hamburg University of Technology, Hamburg, Germany, and the Dr.Sc. degree from Swiss Federal Institute of Technology (ETH) Zurich, Switzerland.

From 2010 to 2015, he was a Research Scientist with the Institute for Infocomm Research, A*STAR, Singapore. He is currently an Associate Professor with the School of Electronic Science and Engineering, Nanjing University. His research interests include next-generation wireless communication networks, deep learning, and mathematical optimization techniques. He was honored with the Dengfeng Scholars Program, Nanjing University, in 2015, the 2009 Chinese Government Award for Outstanding Self-Financed Students Abroad, and the IEEE Globecom 2008 Best Paper Award.

Furao Shen (Member, IEEE) received the B.Sc. and M.Sc. degrees in mathematics from Nanjing University, Nanjing, China, in 1995 and 1998, respectively, and the Ph.D. degree from Tokyo Institute of Technology, Tokyo, Japan, in 2006. He is currently a Full Professor with the School of Artificial Intelligence, Nanjing University. His current research interests include neural computing and robotic intelligence.

Jingon Joung (Senior Member, IEEE) received the B.S. degree in radio communication engineering from Yonsei University, Seoul, South Korea, in 2001, and the M.S. and Ph.D. degrees in electrical engineering and computer science from KAIST, Daejeon, South Korea, in 2003 and 2007, respectively.

He was a Post-Doctoral Fellow with KAIST and UCLA, CA, USA, in 2007 and 2008, respectively. He was a Scientist with the Institute for Infocomm Research, Singapore, from 2009 to 2015, and joined Chung-Ang University (CAU), Seoul, in 2016, as a Faculty Member. He is currently a Professor with the School of Electrical and Electronics Engineering, CAU, where he is also the Principal Investigator of the Intelligent Wireless Systems Laboratory. His research interests include signal processing, numerical analysis, and algorithms.

Dr. Joung was recognized as an Exemplary Reviewer of IEEE COMMUNICATIONS LETTERS in 2012 and IEEE WIRELESS COMMUNICATIONS LETTERS from 2012 to 2014 and in 2019. He served as a Guest Editor for IEEE ACCESS in 2016. He served on the editorial board for *APSIPA Transactions on Signal and Information Processing* from 2014 to 2019, served as a Guest Editor for *Electronics* in 2019, and served as an Associate Editor for IEEE TRANSACTIONS ON VEHICULAR TECHNOLOGY from 2018 to 2023 (Top Editor 2021). He is an inventor of a Space-Time Line Code (STLC) that is a fully symmetric scheme to a space-time block code.

Sumei Sun (Fellow, IEEE) is currently the Executive Director of the Institute for Infocomm Research (I^2R), Agency for Science, Technology, and Research (A*STAR), Singapore. She also holds an adjunct appointment with the National University of Singapore and joint appointment with Singapore Institute of Technology as a Full Professor. Her current research interests include next-generation wireless communications, joint communication-sensing-computing-control design, the Industrial Internet of Things, applied deep learning, and artificial intelligence. She was the Editor-in-Chief of IEEE OPEN JOURNAL OF VEHICULAR TECHNOLOGY from 2019 to 2023. She is a member of the IEEE Vehicular Technology Society Board of Governors (2022–2024) and a fellow of the Academy of Engineering Singapore.

Authorized licensed use limited to: Nanjing University. Downloaded on March 10,2026 at 07:06:34 UTC from IEEE Xplore. Restrictions apply.